

International Journal of Modern Physics B
© World Scientific Publishing Company

**AC CONDUCTIVITY OF GRAPHENE:
FROM TIGHT-BINDING MODEL TO
2 + 1-DIMENSIONAL QUANTUM ELECTRODYNAMICS**

V.P. GUSYNIN

*Bogolyubov Institute for Theoretical Physics,
14-b Metrologicheskaya Str., Kiev, 03680, Ukraine
vgusynin@bitp.kiev.ua*

S.G. SHARAPOV

*Department of Physics and Astronomy, McMaster University,
Hamilton, Ontario, L8S 4M1, Canada
Department of Physics, Western Illinois University,
Macomb, IL 61455, USA
sharapov@bitp.kiev.ua*

J.P. CARBOTTE

*Department of Physics and Astronomy, McMaster University,
Hamilton, Ontario, L8S 4M1, Canada
carbotte@mcmaster.ca*

Received Day Month Year

Revised Day Month Year

We consider the relationship between the tight-binding Hamiltonian of the two-dimensional honeycomb lattice of carbon atoms with nearest neighbor hopping only and the 2 + 1 dimensional Hamiltonian of quantum electrodynamics which follows in the continuum limit. We pay particular attention to the symmetries of the free Dirac fermions including spatial inversion, time reversal, charge conjugation and chirality. We illustrate the power of such a mapping by considering the effect of the possible symmetry breaking which corresponds to the creation of a finite Dirac mass, on various optical properties. In particular, we consider the diagonal AC conductivity with emphasis on how the finite Dirac mass might manifest itself in experiment. The optical sum rules for the diagonal and Hall conductivities are discussed.

Keywords: Graphene; Dirac theory; chirality; symmetry

Preprint: NSF-KITP-07-126

2 *V.P. GUSYNIN, S.G. SHARAPOV, J.P. CARBOTTE***1. Introduction**

A single sheet of carbon atoms tightly packed into a two-dimensional (2D) honeycomb lattice is called graphene. The band structure of graphene consists approximately of a valence (full) and conduction (empty) band both conical in shape with vertex meeting at a point called a Dirac point. There are two inequivalent pairs of such cones. This model, which is based on the continuum limit of tight-binding bands can adequately describe low energy phenomena. Deviations from simple cones can become important however near the ends of the bands where additional details of the tight-binding bands need to be considered. An example of the need to go beyond the continuum approximation, which will be considered in this review, is a discussion of optical sum rules which involve the integration of the optical conductivity or closely related quantity over all energies within the band. An important aspect of the graphene problem is that it can be mapped, in the continuum approximation, into the Hamiltonian of 2 + 1 dimensional quantum electrodynamics (QED₂₊₁) with Dirac fermions. It is remarkable that historically this field theoretical view of graphene started 20 years before¹ its actual discovery² and has motivated theoretical work on a condensed-matter realization of the parity anomaly,^{3,4,5} the renormalization group approach in this system,^{6,7} and nonperturbative dynamics of the generation of an excitonic-like gap in graphene.^{8,9} The interest in Dirac fermions in condensed matter theory was also related to studies of the integer quantum Hall effect (IQHE).¹⁰ Nowadays graphene inspires work on the fractionalization of fermions^{11,12,13} which still waits for the discovery.

The experimental proof of the existence of Dirac fermions in graphene^{14,15} that came from the observation of the theoretically expected unconventional QHE^{16,17,18} with the quantized filling factor

$$\sigma_{xy} = \frac{e^2}{h}\nu, \quad \nu = \pm 2(2n + 1), \quad n = 0, 1, \dots \quad (1)$$

has promoted Dirac fermions from a beautiful theoretical toy to a real object that one day may perform in a "graphenium inside" processor¹⁹ or even sooner become a resistance standard operational above liquid-nitrogen temperature.²⁰ This fortunate situation has created much excitement and it is now possible to consider doing bench top experiment to explore the properties QED₂₊₁. This mapping into QED also means that insight obtained in the study of relativistic fermions can be brought to bare on the study of a solid state system. Examples of relativistic effects that could be studied include the Klein paradox which deals with the perfect transmission of electrons through high potential barrier^{21,22,23} and Zitterbewegung or trembling of the center of a free wave packet.²⁴ The experimental realization of graphene calls for an overview of the theoretical link between the condensed matter lattice description of graphene and its continuum QED₂₊₁ formulation. This should help one judge better which theoretical concepts developed during previous theoretical studies are important for a deeper understanding of the analogies between the behavior of electrons in graphene and in QED₂₊₁.

In this short review we consider in detail this correspondence between a tight-binding lattice model and QED₂₊₁. We concentrate on symmetries of free Dirac fermion problem and the consequences of possible lacking of such symmetries. In particular, we consider spatial inversion, time reversal, charge conjugation and a continuum $U(4)$ symmetry. We explain the difference between 2D Dirac fermions in graphene and the 3D Dirac fermions that are studied in the more familiar QED₃₊₁. In particular, there is a difference in the physical meaning of such an important quantum number as *chirality* in QED₂₊₁ and QED₃₊₁. Because of this and due to the fact that the notion of chirality is now widely used in the literature on graphene (see e.g. Ref. 25), we found that it is useful to explain the similarities and differences of this notion in field theory and graphene.

Another important issue is the possible effect of correlations on various properties of graphene. For example, the new IQHE states^{26,27,28} with the filling factor $\nu = 0, \pm 1$ seen in the strong magnetic field B greater than or equal to 20 T are likely to originate from many-body interactions. In particular, the zero filling factor ($\nu = 0$) state is related to a spin polarized state^{27,28}, while $\nu = \pm 1$ states are probably related to the lifting of sublattice degeneracy. There also exists evidence²⁹ that Coulomb interactions may be partially responsible for an observed increase in the energy difference between second and first Landau levels in fields ~ 18 T. For the conventional case a theorem by Kohn³⁰ based on nearly parabolic bands shows that there should be no such shifts due to correlations, but the theorem may not apply here. An interesting feature of the QED description of graphene is that there is a phenomenon of spontaneous symmetry breaking when the interactions generate a *Dirac mass* or gap. Historically this was exactly the interest in the condensed matter realization of the anomalous properties of *massive* QED₂₊₁, which brought the attention of theoreticians^{1,3,4,5} to graphene before its actual discovery. Now it is an *open question* (see e.g. Ref. 31 for a brief overview and more references are provided below in Sec. 3.6) whether the spontaneous mass generation and symmetry breaking indeed occur in graphene or the observed $\nu = \pm 1$ IQHE states have a different origin. Because the experiment does not yet provide a definitive answer, in this review we discuss the theoretical possibility of breaking the $U(4)$ symmetry of the Lagrangian of graphene by eight Dirac masses. We illustrate how the creation of a finite Dirac mass affects the discrete and continuum symmetries and trace in one case its consequence in the diagonal AC conductivity. It is left to future experiments to verify this theoretical possibility.

Although graphene is only 3 years old, there already exists several popular articles at the introductory^{32,33} and more advanced^{34,35,31} level. Also there is an excellent review article by A.K. Geim and K. Novoselov¹⁹ and a more theoretical review by M.I. Katsnelson and K.S. Novoselov.²³ Because graphene is a basic element of all graphitic forms, all existing literature from late 40's onwards considers graphene as a starting point of the analysis. Particularly useful are the results for carbon nanotubes (see e.g. Refs. 36, 37).

Despite this variety of works on graphene we found that a more formal view

4 V.P. GUSYNIN, S.G. SHARAPOV, J.P. CARBOTTE

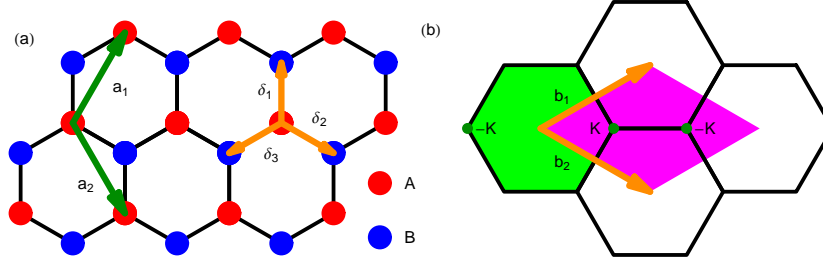


Fig. 1. (Colour online) (a) Graphene hexagonal lattice constructed as a superposition of two triangular lattices A and B, with basis vectors $\mathbf{a}_{1,2}$ for lattice A and vectors δ_i with $i = 1, 2, 3$ connecting A to B. (b) The green hexagon is a Brillouin zone (BZ) and pink diamond is the extended BZ for the honeycomb lattice. The reciprocal lattice vectors are \mathbf{b}_1 and \mathbf{b}_2 .

which can form the bridge between condensed matter and quantum field theory is still missing, and we decided to present it here. The review is organized as follows. In Sec. 2 we introduce the tight-binding model with an external vector potential and obtain expressions for electric current and diamagnetic term. In Sec. 3 we derive the continuum QED₂₊₁ Lagrangian from the tight-binding model of graphene. This allows one to trace the link between the underlying lattice structure of graphene and clarify the physical meaning of the spinor components in the Dirac theory. The physical meaning of chirality in graphene is discussed in Sec. 3.4. In Sec. 3.5 the discrete symmetry operations of the effective Dirac theory are defined in accordance with the discrete symmetries of the lattice model considered in Sec. 2.3. Basing on the discrete symmetries we discuss in Sec. 3.5.4 the difference between massless neutrinos in QED₃₊₁ and quasiparticles in graphene. Eight possible Dirac masses are introduced in Sec. 3.6 and their transformation properties under discrete symmetries are classified. The AC conductivity in zero and finite magnetic field and optical sum rules are considered in Sec. 4. In Sec. 5 we present our conclusions and discuss open questions.

2. Tight-binding description of graphene

2.1. Tight-binding model

The honeycomb lattice can be described in terms of two triangular sublattices, A and B (see Fig. 1 a). A unit cell contains two atoms, one of type A and one of type B. The vectors

$$\mathbf{a}_1 = a\left(\frac{1}{2}, \frac{\sqrt{3}}{2}\right), \quad \mathbf{a}_2 = a\left(\frac{1}{2}, -\frac{\sqrt{3}}{2}\right), \quad (2)$$

shown there are primitive translations, where the lattice constant $a = |\mathbf{a}_1| = |\mathbf{a}_2| = \sqrt{3}a_{CC}$ and a_{CC} is the distance between two nearest carbon atoms. The corresponding reciprocal lattice whose vectors are $\mathbf{b}_1 = \frac{2\pi}{a}(1, 1/\sqrt{3})$ and $\mathbf{b}_2 = \frac{2\pi}{a}(1, -1/\sqrt{3})$ is shown in Fig. 1 b together with the reduced (symmetrical and extended) Brillouin

zone. The reciprocal vectors satisfy the relation $\mathbf{a}_i \cdot \mathbf{b}_j = 2\pi\delta_{ij}$.

Any A atom at the position $\mathbf{n} = \mathbf{a}_1 n_1 + \mathbf{a}_2 n_2$, where n_1, n_2 are integers, is connected to its nearest neighbors on B sites by the three vectors $\boldsymbol{\delta}_i$:

$$\boldsymbol{\delta}_1 = (\mathbf{a}_1 - \mathbf{a}_2)/3, \quad \boldsymbol{\delta}_2 = \mathbf{a}_1/3 + 2\mathbf{a}_2/3, \quad \boldsymbol{\delta}_3 = -\boldsymbol{\delta}_1 - \boldsymbol{\delta}_2 = -2\mathbf{a}_1/3 - \mathbf{a}_2/3. \quad (3)$$

Besides translations, the symmetry group of honeycomb lattice includes rotations (R and R^{-1}) on $\pm 2\pi/3$ and mirror reflections (Y_1, Y_2, Y_3) about planes passing through the center and three hexagon vertices. Together the rotations and reflections form a nonabelian group C_{3v} with 6 elements. Their explicit matrix representation may be defined by matrices giving the transformations of the basis vectors \mathbf{a}_1 and \mathbf{a}_2 ,

$$E = \begin{pmatrix} 1 & 0 \\ 0 & 1 \end{pmatrix}, \quad R = \begin{pmatrix} -1 & -1 \\ 1 & 0 \end{pmatrix}, \quad R^{-1} = \begin{pmatrix} 0 & 1 \\ -1 & -1 \end{pmatrix}, \\ Y_1 = \begin{pmatrix} -1 & 0 \\ 1 & 1 \end{pmatrix}, \quad Y_2 = \begin{pmatrix} 1 & 1 \\ 0 & -1 \end{pmatrix}, \quad Y_3 = \begin{pmatrix} 0 & -1 \\ -1 & 0 \end{pmatrix}. \quad (4)$$

In addition there is a reflection Z in the plane of the sheet (changes $\mathbf{a}_i \rightarrow -\mathbf{a}_i$, followed by the translation by one of the vectors $3\boldsymbol{\delta}_i$) and, accordingly, combinations of Z with any of the above operations. All these operations do not interchange A- and B-type atoms. The one-electron eigenfunctions can be classified according to the subgroup (E, Z) whether the states are even (σ states) or odd (π states) under reflection Z . There are also operations which interchange A and B atoms, for example, reflections X_1, X_2, X_3 in mirror planes perpendicular to the corresponding Y_i planes. They are symmetry operations when accompanied by some fractional translations.³⁸ The rotation and rotation-reflection operations (leaving aside Z reflection) form the point-group of graphene which contains 12 elements. The effect of group operations G on a function of the coordinates is defined as $\psi'(\mathbf{r}) = \psi(G^{-1}\mathbf{r}) = T(G)\psi(\mathbf{r})$, and it allows one to determine the irreducible representations for graphene. In particular, one should note that the subgroup (4) has a two-dimensional spinor representation which we use below. Full consideration of the symmetry group of graphene was made in Refs. 38, 39.

The carbon atoms in graphene plane are connected by strong covalent σ -bonds due to the sp^2 hybridization of the atomic $2s, 2p_x, 2p_y$ orbitals. The $2p_z$ (π) orbitals are perpendicular to the plane and have a weak overlap. Therefore we start with the simplest tight-binding description for π orbitals of carbon in terms of the Hamiltonian

$$H = -t \sum_{\mathbf{n}, \boldsymbol{\delta}_i, \sigma} \left[a_{\mathbf{n}, \sigma}^\dagger \exp\left(\frac{ie}{\hbar c} \boldsymbol{\delta}_i \mathbf{A}\right) b_{\mathbf{n}+\boldsymbol{\delta}_i, \sigma} + \text{c.c.} \right], \quad (5)$$

where t is the nearest neighbor hopping parameter, $a_{\mathbf{n}, \sigma}$ and $b_{\mathbf{n}+\boldsymbol{\delta}_i, \sigma}$ are the Fermi operators of electrons with spin $\sigma = \uparrow, \downarrow$ on A and B sublattices, respectively. Since we are interested in the current response, the vector potential \mathbf{A} is introduced in the Hamiltonian (5) by means of the Peierls substitution $a_{\mathbf{n}, \sigma}^\dagger b_{\mathbf{m}, \sigma} \rightarrow$

6 *V.P. GUSYNIN, S.G. SHARAPOV, J.P. CARBOTTE*

$a_{\mathbf{n},\sigma}^\dagger \exp\left(-\frac{ie}{\hbar c} \int_{\mathbf{m}}^{\mathbf{n}} \mathbf{A} d\mathbf{r}\right) b_{\mathbf{m},\sigma}$ that introduces the phase factor $\exp\left(\frac{ie}{\hbar c} \boldsymbol{\delta}_i \mathbf{A}\right)$ in the hopping term (see Ref. 40 for a review). We keep Planck constant \hbar and the velocity of light c , but set $k_B = 1$. The charge of electron is $-e < 0$. Note that we consider a 2D model. The experiment shows that graphene, in order to exist without a substrate, spreads itself out of the 2D plane.⁴¹

Expanding the Hamiltonian (5) to the second order in the vector potential, one has

$$H = H_0 - \sum_{\mathbf{n}} \left[\frac{1}{c} \mathbf{A}(\mathbf{n}) \mathbf{j}(\mathbf{n}) - \frac{1}{2c^2} A_\alpha(\mathbf{n}) \tau_{\alpha\beta}(\mathbf{n}) A_\beta(\mathbf{n}) \right], \quad \alpha, \beta = 1, 2. \quad (6)$$

The total current density operator is obtained by differentiating Eq. (6) with respect to $A_\alpha(\mathbf{n})$,

$$j_\alpha(\mathbf{n}) = -\frac{\partial H}{\partial (A_\alpha/c)} = j_\alpha^P(\mathbf{n}) - \tau_{\alpha\beta}(\mathbf{n}) A_\beta(\mathbf{n})/c, \quad (7)$$

and consists of the usual paramagnetic part,

$$j_\alpha^P(\mathbf{n}) = \frac{ite}{\hbar} \sum_{\boldsymbol{\delta}_i, \sigma} (\delta_i)_\alpha \left[a_{\mathbf{n},\sigma}^\dagger b_{\mathbf{n}+\boldsymbol{\delta},\sigma} - b_{\mathbf{n}+\boldsymbol{\delta},\sigma}^\dagger a_{\mathbf{n},\sigma} \right], \quad (8)$$

and diamagnetic part,

$$\tau_{\alpha\beta}(\mathbf{n}) = \frac{\partial^2 H}{\partial (A_\alpha/c) \partial (A_\beta/c)} = \frac{te^2}{\hbar^2} \sum_{\boldsymbol{\delta}_i, \sigma} (\delta_i)_\alpha (\delta_i)_\beta \left[a_{\mathbf{n},\sigma}^\dagger b_{\mathbf{n}+\boldsymbol{\delta},\sigma} + b_{\mathbf{n}+\boldsymbol{\delta},\sigma}^\dagger a_{\mathbf{n},\sigma} \right]. \quad (9)$$

We stress that to obtain the correct form of the current (8) and the diamagnetic part (9), the Peierls substitution has to be made in the initial Hamiltonian (5) or its momentum representation (see Eq. (10) below) rather than after the diagonalization of these Hamiltonians is made (see Ref. 42 and references therein). We will return to the paramagnetic and diamagnetic terms of the interacting Hamiltonian (6) later when we discuss coupling to the vector potential in Sec. 3.2 and the sum rules in Sec. 4.4. For now we consider the noninteracting Hamiltonian H_0 .

2.2. Spinor representation of the noninteracting Hamiltonian

In the momentum representation the Hamiltonian H_0 reads

$$H_0 = \sum_{\sigma} \int_{BZ} \frac{d^2k}{(2\pi)^2} \Upsilon_{\sigma}^\dagger(\mathbf{k}) \mathcal{H}_0 \Upsilon_{\sigma}(\mathbf{k}), \quad \mathcal{H}_0 = \begin{pmatrix} 0 & \phi(\mathbf{k}) \\ \phi^*(\mathbf{k}) & 0 \end{pmatrix} \quad (10)$$

with $\phi(\mathbf{k}) = -t \sum_{\boldsymbol{\delta}_i} e^{i\mathbf{k}\boldsymbol{\delta}_i} \equiv -\epsilon(\mathbf{k}) e^{i\varphi(\mathbf{k})}$. In the basis (2) we get

$$\begin{aligned} \phi(\mathbf{k}) &= -te^{i\mathbf{k}(\mathbf{a}_1 - \mathbf{a}_2)/3} \left[1 + e^{i\mathbf{k}\mathbf{a}_2} + e^{-i\mathbf{k}\mathbf{a}_1} \right] \\ &= -t \left[\exp\left(i \frac{k_y a}{\sqrt{3}}\right) + \exp\left(-i \frac{k_y a}{2\sqrt{3}}\right) 2 \cos \frac{k_x a}{2} \right] \end{aligned} \quad (11)$$

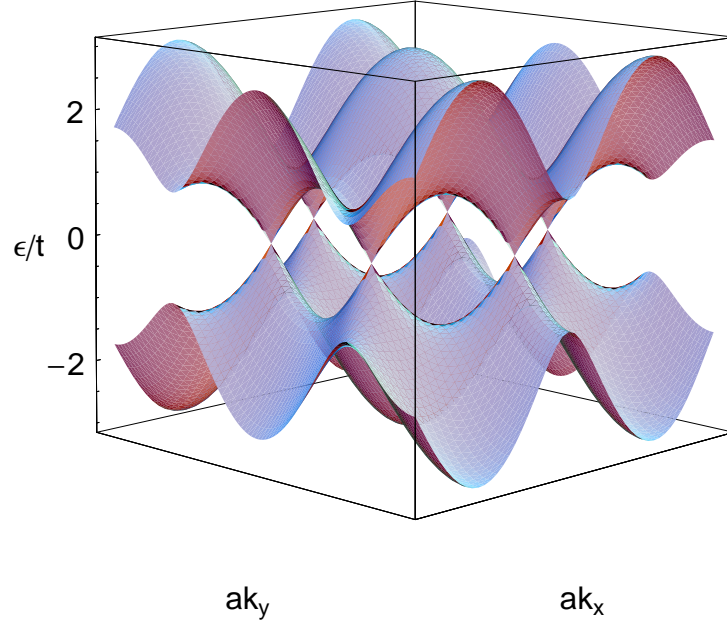


Fig. 2. (Colour online) The energy band structure of graphene. Valence and conduction bands meet at six \mathbf{K} points.

and

$$\epsilon(\mathbf{k}) = t \sqrt{1 + 4 \cos^2 \frac{k_x a}{2} + 4 \cos \frac{k_x a}{2} \cos \frac{\sqrt{3} k_y a}{2}}. \quad (12)$$

Accordingly, because the graphene structure contains two atoms per unit cell (two sublattices), the spectrum of quasiparticles excitations has two branches (bands) with the dispersion⁴³ $E_{\pm} = \pm \epsilon(\mathbf{k})$ shown in Fig. 2. In Eq. (10) we introduced the spinors

$$\Upsilon_{\sigma}(\mathbf{k}) = \begin{pmatrix} a_{\sigma}(\mathbf{k}) \\ b_{\sigma}(\mathbf{k}) \end{pmatrix} \quad (13)$$

with the operator $\Upsilon_{\sigma}(\mathbf{k})$ being the Fourier transform of the spinor $\Upsilon_{\sigma}(\mathbf{n}) = \begin{pmatrix} a_{\mathbf{n},\sigma} \\ b_{\mathbf{n},\sigma} \end{pmatrix}$:

$$\Upsilon_{\sigma}(\mathbf{n}) = \sqrt{S} \int_{BZ} \frac{d^2 \mathbf{k}}{(2\pi)^2} e^{i\mathbf{k}\mathbf{n}} \Upsilon_{\sigma}(\mathbf{k}). \quad (14)$$

Here $S = \sqrt{3}a^2/2$ is the area of a unit cell and the integration in Eqs. (10) and (14) goes over the extended rhombic Brillouin zone (BZ). We also add to H_0 the Zeeman term and the chemical potential

$$H_Z = - \sum_{\sigma} \mu_{\sigma} \int_{BZ} \frac{d^2 k}{(2\pi)^2} \Upsilon_{\sigma}^{\dagger}(\mathbf{k}) \Upsilon_{\sigma}(\mathbf{k}) \quad (15)$$

8 *V.P. GUSYNIN, S.G. SHARAPOV, J.P. CARBOTTE*

with $\mu_\sigma = \mu - \sigma g/2\mu_B B$, where $\mu_B = e\hbar/(2m_e c)$ is the Bohr magneton, and g is the Lande factor. We count the Zeeman energy from the chemical potential μ , so that our subsequent consideration is based on the grand canonical ensemble.

The corresponding imaginary time Green's function (GF) is defined as a thermal average

$$G_\sigma(\tau_1 - \tau_2, \mathbf{n}_1 - \mathbf{n}_2) = -\langle T_\tau \Upsilon_\sigma(\tau_1, \mathbf{n}_1) \Upsilon_\sigma^\dagger(\tau_2, \mathbf{n}_2) \rangle \quad (16)$$

and its Fourier transform is

$$G_\sigma(\tau_1 - \tau_2, \mathbf{n}_1 - \mathbf{n}_2) = ST \sum_n \int_{BZ} \frac{d^2 \mathbf{k}}{(2\pi)^2} G_\sigma(i\omega_n, \mathbf{k}) \exp[-i\omega_n(\tau_1 - \tau_2) + i\mathbf{k}(\mathbf{n}_1 - \mathbf{n}_2)] \quad (17)$$

with

$$G_\sigma(i\omega_n, \mathbf{k}) = \frac{(i\omega_n + \mu_\sigma) \hat{I} + \tau_+ \phi(\mathbf{k}) + \tau_- \phi^*(\mathbf{k})}{(i\omega_n + \mu_\sigma)^2 - \epsilon^2(\mathbf{k})}, \quad \omega_n = \pi(2n + 1)T, \quad (18)$$

where the matrices $\tau_\pm = (\tau_1 \pm i\tau_2)/2$ made from Pauli matrices, operate in the sublattice space. The GF (18) describes the electron- and hole-like excitations with the energies $E_\pm(\mathbf{k}) = \pm\epsilon(\mathbf{k}) - \mu_\sigma$, respectively.

The dispersion $\epsilon(\mathbf{k})$ near the six \mathbf{K} points $\pm 2\pi/a(1/3, 1/\sqrt{3})$, $\pm 2\pi/a(2/3, 0)$, $\pm 2\pi/a(1/3, -1/\sqrt{3})$ at the corners of the hexagonal BZ (see Fig. 2) is linear,⁴³ $E_\pm(\mathbf{p}) = \pm\hbar v_F |\mathbf{p}| - \mu_\sigma$ (see Fig. 3 (a) in Sec. 3.6), where the wave vector $\mathbf{p} = (p_1, p_2)$ is now measured from the \mathbf{K} points and the Fermi velocity is $v_F = \sqrt{3}ta/(2\hbar)$. Its experimental value^{14,15} is $v_F \approx 10^6$ m/s (see also Ref. 44 for more recent values of v_F and t). Since only two \mathbf{K} points are inequivalent, in what follows, we select them to be $\mathbf{K}_\pm = \pm 2\pi/a(2/3, 0)$ (see Fig. 1 b), so that they are inside the extended BZ. The degeneracy of the two \mathbf{K}_\pm points is protected by the point-group symmetry of the hexagonal lattice.

2.3. Discrete symmetries of the tight-binding Hamiltonian

The \mathbf{K}_\pm points in single layer graphene are stable against perturbations which preserve the discrete spacetime inversion symmetry and which do not mix the \mathbf{K}_\pm points.⁴⁵ We consider these symmetries for the tight-binding model and define below the corresponding discrete symmetry operations for the effective QED₂₊₁ theory of graphene. A topological stability for the appearance of massless Dirac fermions was studied in Ref. 46, and in Sec. 2.3.3 we discuss it.

2.3.1. The spatial inversion \mathcal{P}

Choosing the center of symmetry to be the center of the hexagon³⁹ in Fig. 1 a, we observe that the spatial inversion $\mathcal{P}: (x, y) \rightarrow (-x, -y)$ would be the symmetry of the system if one also exchanges A and B atoms, i.e.

$$a_{\mathbf{n},\sigma} \rightarrow \mathcal{P} a_{\mathbf{n},\sigma} \mathcal{P}^{-1} = b_{-\mathbf{n},\sigma} \quad b_{\mathbf{n},\sigma} \rightarrow \mathcal{P} b_{\mathbf{n},\sigma} \mathcal{P}^{-1} = a_{-\mathbf{n},\sigma}. \quad (19)$$

As we will discuss in Sec. 3.5, the definition of \mathcal{P} is different from that commonly used in QED₂₊₁.¹² In momentum space \mathcal{P} acts as follows

$$a_\sigma(\mathbf{k}) \rightarrow \mathcal{P}a_\sigma(\mathbf{k})\mathcal{P}^{-1} = b_\sigma(-\mathbf{k}), \quad b_\sigma(\mathbf{k}) \rightarrow \mathcal{P}b_\sigma(\mathbf{k})\mathcal{P}^{-1} = a_\sigma(-\mathbf{k}), \quad (20)$$

i.e. it reverses the sign of the momentum $\mathbf{k} \rightarrow -\mathbf{k}$ and exchanges \mathbf{K} points. For the spinors $\Upsilon_\sigma(\mathbf{k})$, the action of \mathcal{P} is defined as

$$\Upsilon_\sigma(\mathbf{k}) \longrightarrow \mathcal{P}\Upsilon_\sigma(\mathbf{k})\mathcal{P}^{-1} = \tau_1\Upsilon_\sigma(-\mathbf{k}). \quad (21)$$

One can easily check that the noninteracting Hamiltonian H_0 is invariant under \mathcal{P}

$$H_0 \longrightarrow \mathcal{P}H_0\mathcal{P}^{-1} = H_0 \quad (22)$$

because the Hamiltonian density \mathcal{H}_0 satisfies the condition

$$\tau_1\mathcal{H}_0(\mathbf{k})\tau_1 = \mathcal{H}_0(-\mathbf{k}). \quad (23)$$

However, if one assumes that the densities of particles on the A and B sublattices are different, i.e. that

$$\begin{aligned} H_1 &= \sum_\sigma \int_{BZ} \frac{d^2\mathbf{k}}{(2\pi)^2} [m_a a_\sigma^\dagger(\mathbf{k})a_\sigma(\mathbf{k}) + m_b b_\sigma^\dagger(\mathbf{k})b_\sigma(\mathbf{k})] \\ &= \sum_\sigma \int_{BZ} \frac{d^2\mathbf{k}}{(2\pi)^2} \Upsilon_\sigma^\dagger(\mathbf{k}) [m_+ \tau_0 + m_- \tau_3] \Upsilon_\sigma(\mathbf{k}) \end{aligned} \quad (24)$$

with $m_+ = (m_a + m_b)/2$ [τ_0 is 2×2 unit matrix] and $m_- = (m_a - m_b)/2$ such term would break the inversion symmetry by swapping now inequivalent sublattices:

$$H_1 \longrightarrow \mathcal{P}H_1\mathcal{P}^{-1} = \sum_\sigma \int_{BZ} \frac{d^2k}{(2\pi)^2} [m_b a_\sigma^\dagger(\mathbf{k})a_\sigma(\mathbf{k}) + m_a b_\sigma^\dagger(\mathbf{k})b_\sigma(\mathbf{k})] \quad (25)$$

or in spinor notation

$$H_1 \longrightarrow \mathcal{P}H_1\mathcal{P}^{-1} = \sum_\sigma \int_{BZ} \frac{d^2k}{(2\pi)^2} \Upsilon_\sigma^\dagger(\mathbf{k}) (m_+ \tau_0 - m_- \tau_3) \Upsilon_\sigma(\mathbf{k}). \quad (26)$$

One can see that the term with m_+ that corresponds to the same carrier density on A and B sublattices can be absorbed in the chemical potential μ , and the carrier imbalance term with m_- is parity breaking. In practice, it has been suggested that one can introduce a Dirac mass term by placing the graphene sheet on a substrate made of hexagonal boron nitride. In this circumstance the two carbon sublattices become inequivalent because of its interaction with the substrate. A recent band structure calculation⁴⁷ for such a configuration has given a gap of about 53 meV.

2.3.2. Time reversal \mathcal{T}

The time-reversal operation, $t \rightarrow -t$ changes the signs of the momentum and spin leaving the sign of coordinates unchanged:⁴⁸

$$\begin{pmatrix} a_+(\mathbf{k}) \\ a_-(\mathbf{k}) \end{pmatrix} \rightarrow \mathcal{T} \begin{pmatrix} a_+(\mathbf{k}) \\ a_-(\mathbf{k}) \end{pmatrix} \mathcal{T}^{-1} = \begin{pmatrix} a_-(-\mathbf{k}) \\ -a_+(-\mathbf{k}) \end{pmatrix} = i\sigma_2 \begin{pmatrix} a_+(-\mathbf{k}) \\ a_-(-\mathbf{k}) \end{pmatrix}, \quad (27)$$

10 V.P. GUSYNIN, S.G. SHARAPOV, J.P. CARBOTTE

The operator $b_{\pm}(\mathbf{k})$ obeys the same rule, and $a_{\pm}^{\dagger}(\mathbf{k})$, $b_{\pm}^{\dagger}(\mathbf{k})$ transform as follows

$$\left(a_{+}^{\dagger}(\mathbf{k}) \ a_{-}^{\dagger}(\mathbf{k}) \right) \rightarrow \mathcal{T} \left(a_{+}^{\dagger}(\mathbf{k}) \ a_{-}^{\dagger}(\mathbf{k}) \right) \mathcal{T}^{-1} = \left(a_{+}^{\dagger}(\mathbf{k}) \ a_{-}^{\dagger}(\mathbf{k}) \right) (-i\sigma_2). \quad (28)$$

To invert the direction of time, the operator \mathcal{T} has to be antiunitary. The action of \mathcal{T} on the sublattice spinors is given by

$$\Upsilon(\mathbf{k}) \rightarrow \mathcal{T}\Upsilon(\mathbf{k})\mathcal{T}^{-1} = i\sigma_2\Upsilon(-\mathbf{k}), \quad (29)$$

where σ_2 acts on the spin indices of the spinor $\Upsilon_{\sigma}(\mathbf{k})$.

One can check that the noninteracting Hamiltonian H_0 is invariant under \mathcal{T}

$$H_0 \rightarrow \mathcal{T}H_0\mathcal{T}^{-1} = H_0 \quad (30)$$

because \mathcal{H}_0 satisfies the condition

$$\tau_0\mathcal{H}_0^*(\mathbf{k})\tau_0 = \mathcal{H}_0(-\mathbf{k}). \quad (31)$$

Since a fixed external magnetic field breaks time reversal symmetry, both the Hamiltonian (5) which includes this field and the Zeeman term (15) break it. On the other hand, the Hamiltonian H_1 given by (24) is invariant under time reversal, but if we consider spin dependent masses $m_{a,b,\sigma}$, it will also break this symmetry.

The presence of combined \mathcal{PT} symmetry enforces a condition on \mathcal{H}_0 :

$$\tau_1\mathcal{H}_0^*(\mathbf{k})\tau_1 = \mathcal{H}_0(\mathbf{k}) \quad (32)$$

or in matrix components: $\mathcal{H}_0^{11} = \mathcal{H}_0^{22}$ and $\mathcal{H}_0^{12} = \mathcal{H}_0^{21*}$. One can say that the first equality forbids $m_{-}\tau_3$ terms in the Hamiltonian protecting \mathbf{K}_{\pm} points when they are not mixed.⁴⁵ The energy spectrum is $E = \mathcal{H}_0^{11} \pm |\mathcal{H}_0^{12}|$. For $\mathcal{H}_0^{11} = \text{const}$, a constant term can be absorbed in the chemical potential, so that \mathcal{PT} symmetry results in the symmetry of the spectrum similarly to the relation (33) considered below.

2.3.3. Particle-hole symmetry of the spectrum and stability of Fermi point

The Hamiltonian $\mathcal{H}_0(\mathbf{k})$ also satisfies two other relations^{49,11,46,50} (see also the end of Sec. 3.4)

$$\tau_3\mathcal{H}_0(\mathbf{k})\tau_3 = -\mathcal{H}_0(\mathbf{k}) \quad (33)$$

and

$$\tau_2\mathcal{H}_0^*(\mathbf{k})\tau_2 = -\mathcal{H}_0(\mathbf{k}). \quad (34)$$

It is easy to check that they guarantee that if there is a state $|\psi\rangle$ with energy E , then the states $\tau_3|\psi\rangle$ and $\tau_2|\psi\rangle^*$ correspond to the energy $-E$ which implies that the energy bands are symmetric about $E = 0$. We note that while the parity breaking term $m_{-}\Upsilon^{\dagger}\tau_3\Upsilon$ obviously violates the condition (33), the more general condition (34) is still satisfied. Indeed, even for $m_{-} \neq 0$ the spectrum is symmetric about $E = 0$: $E(\mathbf{k}) = \pm\sqrt{m_{-}^2 + |\phi(\mathbf{k})|^2}$. In order for the Fermi point $E(\mathbf{k} = 0) = 0$

to exist, we must require the relation (33) which is a necessary but not sufficient condition for its existence. The existence and stability of the Fermi point is dictated by topology in momentum space⁵¹ that is by nonzero topological invariant (winding number) which is expressed analytically as

$$N = \oint_C \frac{d\mathbf{k}}{4\pi i} \text{tr}[\sigma_3 H^{-1}(\mathbf{k}) \partial_{\mathbf{k}} H(\mathbf{k})]. \quad (35)$$

Here the integral is taken over an arbitrary contour C around one of the \mathbf{K}_{\pm} points and tr is the trace over sublattice indices. For the Hamiltonian \mathcal{H}_0 given by (10) the topological invariant can be rewritten in the form

$$N = \frac{1}{4\pi i} \oint_C \frac{\phi(\mathbf{k}) d\phi^*(\mathbf{k}) - \phi^*(\mathbf{k}) d\phi(\mathbf{k})}{|\phi(\mathbf{k})|^2}. \quad (36)$$

For \mathbf{K}_{\pm} points this gives $N(\mathbf{K}_{\pm}) = \pm 1$. On the other hand, when the spectrum becomes gapped, the topological invariant $N = 0$ and the Fermi surfaces disappear. This can happen because the total topological charge at two \mathbf{K}_{\pm} points $N = 0$. The trivial total topological charge of the Fermi surfaces allows for their annihilation, which occurs when the energy spectrum becomes fully gapped.

Now we come to the question of topological stability of the Dirac points with respect to the presence of the other hopping terms.⁴⁶

The next neighbor (intrasublattice) hopping considered, for example, in Ref. 52, introduces only the diagonal term in the Hamiltonian \mathcal{H}_0 in Eq. (10) which eliminates the particle-hole symmetry of original energy bands and for which small deviations from \mathbf{K}_{\pm} can be absorbed in the chemical potential.¹⁸ Thus, we address here the role of the diagonal transfer (third neighbor hopping) t' which is described by

$$H_{t'} = -t' \sum_{\mathbf{n}, \sigma} a_{\mathbf{n}, \sigma}^{\dagger} b_{\mathbf{n} - 2\delta_1} + \text{c.c.} \quad (37)$$

Accordingly, in the presence of $H_{t'}$, Eq. (11) for $\phi(\mathbf{k})$ takes the form

$$\begin{aligned} \phi(\mathbf{k}) &= -t \sum_{\delta_i} e^{i\mathbf{k}\delta_i} - t' e^{-2i\mathbf{k}\delta_1} \\ &= -t e^{i\mathbf{k}\delta_1} \left[1 + e^{i\mathbf{k}(\delta_2 - \delta_1)} + e^{i\mathbf{k}(\delta_3 - \delta_1)} + \frac{t'}{t} e^{-3i\mathbf{k}\delta_1} \right]. \end{aligned} \quad (38)$$

Using the relations (3) we write

$$\phi(\mathbf{k}) = -t e^{i\mathbf{k}\delta_1} \left[1 + e^{ik_2} + e^{-ik_1} \left(1 + \frac{t'}{t} e^{ik_2} \right) \right] \equiv -t e^{i\mathbf{k}\delta_1} \bar{\phi}(\mathbf{k}), \quad (39)$$

where we introduced the notations $k_1 = \mathbf{k}\mathbf{a}_1$, $k_2 = \mathbf{k}\mathbf{a}_2$. Note that these variables change from $-\pi$ to π . In the complex plane $\bar{\phi}(\mathbf{k})$ delineates a circle centered at $C_0 = 1 + e^{ik_2}$ with a radius $r = \sqrt{1 + 2(t'/t) \cos k_2 + (t'/t)^2}$ when k_1 is changed from $-\pi$ to π for a fixed value k_2 . In order to have a Dirac cone, the circle must cross the origin of coordinates. This is guaranteed for the values $-3 \leq t'/t < 1$. Thus, the Dirac cone is stable against additional interactions, diagonal hopping, when the last

condition is satisfied. The appearance of gapless Dirac fermions is not accidental to the honeycomb lattice, but is rather generic for a class of two-dimensional lattices that interpolate between square ($t' = t$) and π -flux ($t' = -t$) lattices. This indicates a certain robustness of the topological quantum number.

3. QED₂₊₁ description of graphene

3.1. Noninteracting Dirac Hamiltonian

Around two inequivalent \mathbf{K}_\pm points, where $\epsilon(\mathbf{K}_\pm) = 0$, the function (11) can be expanded as $\phi(\mathbf{K}_\pm + \mathbf{p}) = \pm \hbar v_F (p_1 \mp i p_2)$, so that the Hamiltonian (10) is linearized^{1,53}

$$H_0 = \sum_{\sigma} \int_{DC} \frac{d^2 p}{(2\pi)^2} \left[\Upsilon_{\sigma}^{\dagger}(\mathbf{K}_+ + \mathbf{p}) \mathcal{H}_{\mathbf{K}_+}(\mathbf{p}) \Upsilon_{\sigma}(\mathbf{K}_+ + \mathbf{p}) + \Upsilon_{\sigma}^{\dagger}(\mathbf{K}_- + \mathbf{p}) \mathcal{H}_{\mathbf{K}_-}(\mathbf{p}) \Upsilon_{\sigma}(\mathbf{K}_- + \mathbf{p}) \right], \quad (40)$$

with the Hamiltonian densities for \mathbf{K}_\pm points

$$\mathcal{H}_{\mathbf{K}_+} = \hbar v_F (\tau_1 p_1 + \tau_2 p_2), \quad \mathcal{H}_{\mathbf{K}_-} = \hbar v_F (-\tau_1 p_1 + \tau_2 p_2). \quad (41)$$

The integration in Eq. (40) is done over the Dirac cone (DC) and the energy cutoff which preserves the number of states is

$$W = \hbar v_F \sqrt{\frac{\Omega_B}{2\pi}} = \frac{\hbar v_F}{a} \sqrt{\frac{4\pi}{\sqrt{3}}} = \sqrt{\pi \sqrt{3} t} \approx 2.33t, \quad (42)$$

where $\Omega_B = (2\pi)^2/S$ is BZ area.

It is convenient to use a 4-component spinor $\Psi_{\sigma}(\mathbf{p})$ made from the two spinors for \mathbf{K}_\pm points. When the spinors $\Upsilon_{\sigma}(\mathbf{K}_\pm + \mathbf{p})$ are combined into one, we exchange the sublattices in the spinor for \mathbf{K}_- point,^a so that

$$\Psi_{\sigma}(\mathbf{p}) = \begin{pmatrix} \psi_{\mathbf{K}_+, \sigma}(\mathbf{p}) \\ \psi_{\mathbf{K}_-, \sigma}(\mathbf{p}) \end{pmatrix} = \begin{pmatrix} a_{\sigma}(\mathbf{K}_+ + \mathbf{p}) \\ b_{\sigma}(\mathbf{K}_+ + \mathbf{p}) \\ b_{\sigma}(\mathbf{K}_- + \mathbf{p}) \\ a_{\sigma}(\mathbf{K}_- + \mathbf{p}) \end{pmatrix}. \quad (43)$$

Accordingly, the Hamiltonian (40) acquires the form

$$H_0 = \hbar v_F \sum_{\sigma} \int_{DC} \frac{d^2 p}{(2\pi)^2} \Psi_{\sigma}^{\dagger}(\mathbf{p}) \begin{pmatrix} K_{+A} & K_{+B} & K_{-B} & K_{-A} \\ 0 & p_x - i p_y & 0 & 0 \\ p_x + i p_y & 0 & 0 & 0 \\ 0 & 0 & 0 & -p_x + i p_y \\ 0 & 0 & -p_x - i p_y & 0 \end{pmatrix} \Psi_{\sigma}(\mathbf{p}) \\ = \hbar v_F \sum_{\sigma} \int_{DC} \frac{d^2 p}{(2\pi)^2} \Psi_{\sigma}^{\dagger}(\mathbf{p}) \mathcal{H}_0(\mathbf{p}) \Psi_{\sigma}(\mathbf{p}), \quad \mathcal{H}_0(\mathbf{p}) = \alpha^1 p_1 + \alpha^2 p_2. \quad (44)$$

^aThis allows to use the same Hamiltonian for both \mathbf{K} points, i.e. $\mathcal{H}_{\mathbf{K}_\pm} = \pm \hbar v_F (\tau_1 p_1 + \tau_2 p_2)$ and obtain the standard representation of gamma matrices.

Here the 4×4 matrices $\alpha^{1,2}$ are the first two α matrices out of the three α^i ($i = 1, 2, 3$) matrices

$$\boldsymbol{\alpha} = (\alpha^1, \alpha^2, \alpha^3) = \tilde{\tau}_3 \otimes (\tau_1, \tau_2, \tau_3) = \begin{pmatrix} \boldsymbol{\tau} & 0 \\ 0 & -\boldsymbol{\tau} \end{pmatrix} \quad (45)$$

that anticommute among themselves and with the matrix β :

$$\beta = \tilde{\tau}_1 \otimes I_2 = \begin{pmatrix} 0 & I_2 \\ I_2 & 0 \end{pmatrix}. \quad (46)$$

The irreducible representation of the Dirac algebra in $(2+1)$ dimensions is given by 2×2 matrices and there are two such irreducible representations differing in sign. They are both used in Eq. (44), reflecting the fact that in addition to two degrees of freedom associated with the A and B sublattices, one should also take into account fermions at two distinct \mathbf{K}_{\pm} points. These degrees of freedom are described by $\tilde{\tau}$ matrices that act in the valley (\mathbf{K}_{\pm}) subspace and as a result, we use a 4×4 reducible (in $2+1$ dimensions) representation of the Dirac matrices.

3.2. Lagrangian of graphene

To finish the mapping of the tight-binding model for graphene into QED₂₊₁, we introduce γ matrices and include an external magnetic field. We choose

$$\gamma^0 = \beta, \quad \boldsymbol{\gamma} = \beta \boldsymbol{\alpha} = -i\tilde{\tau}_2 \otimes (\tau_1, \tau_2, \tau_3) = \begin{pmatrix} 0 & -\boldsymbol{\tau} \\ \boldsymbol{\tau} & 0 \end{pmatrix} \quad (47)$$

and introduce the Dirac conjugated spinor $\bar{\Psi}_{\sigma}(\mathbf{p}) = \Psi_{\sigma}^{\dagger}(\mathbf{p})\gamma^0$. The matrices γ^{ν} with $\nu = 0, 1, 2, 3$ satisfy the usual anticommutation relations

$$\{\gamma^{\mu}, \gamma^{\nu}\} = 2g^{\mu\nu}I_4, \quad g^{\mu\nu} = (1, -1, -1, -1), \quad \mu, \nu = 0, 1, 2, 3, \quad (48)$$

but we remind that in QED₂₊₁, we do not use γ^3 in the Dirac representation of the Hamiltonian

$$H_0 = \sum_{\sigma} \int_{DC} \frac{d^2p}{(2\pi)^2} \bar{\Psi}_{\sigma}(\mathbf{p}) \mathcal{H}_0^D(\mathbf{p}) \Psi_{\sigma}(\mathbf{p}),$$

$$\mathcal{H}_0^D(\mathbf{p}) = \gamma^0 \mathcal{H}_0(\mathbf{p}) = \hbar v_F (\gamma^1 p_1 + \gamma^2 p_2). \quad (49)$$

The representation (47) is called the Weyl or chiral representation of γ matrices and because these matrices are 4×4 , one can construct the chiral γ^5 matrix as

$$\gamma^5 = i\gamma^0\gamma^1\gamma^2\gamma^3 = \begin{pmatrix} I_2 & 0 \\ 0 & -I_2 \end{pmatrix} \quad (50)$$

which commutes with the α^i and anticommutes with the γ^{ν} . We note that the chiral representation Eq. (47) by means of the matrix

$$S = \frac{1}{\sqrt{2}} \begin{pmatrix} I & \tau_3 \\ I & -\tau_3 \end{pmatrix}, \quad S^{-1} = \frac{1}{\sqrt{2}} \begin{pmatrix} I & I \\ \tau_3 & -\tau_3 \end{pmatrix}, \quad (51)$$

14 *V.P. GUSYNIN, S.G. SHARAPOV, J.P. CARBOTTE*

translates into another representation

$$\begin{aligned}\gamma^\nu &= \tilde{\tau}_3 \otimes (\tau_3, i\tau_2, -i\tau_1) = \begin{pmatrix} \hat{\gamma}^0 & 0 \\ 0 & \tilde{\gamma}^0 \end{pmatrix}, \begin{pmatrix} \hat{\gamma}^1 & 0 \\ 0 & \tilde{\gamma}^1 \end{pmatrix}, \begin{pmatrix} \hat{\gamma}^2 & 0 \\ 0 & \tilde{\gamma}^2 \end{pmatrix}, \\ \gamma^3 &= \begin{pmatrix} 0 & I \\ -I & 0 \end{pmatrix}, \quad \gamma^5 = \begin{pmatrix} 0 & I \\ I & 0 \end{pmatrix},\end{aligned}\quad (52)$$

which was used in Refs. 8, 17, 54, 55. Note that various researchers used different representations of the Dirac algebra (see e.g. Refs. 1, 6, 9, 56), so that the comparison of the $U(4)$ symmetry breaking terms in terms of the underlying lattice and band structure of graphene is rather complicated. Our choice of the chiral representation of γ matrices in Eq. (47) is motivated by the fact that in this representation, the spinors with a definite chirality are eigenstates of γ^5 which makes the physical interpretation of the chirality quantum number in graphene in Sec. 3.4 more transparent. Another advantage of this representation is that one can make a comparison with some recent works in Refs. 57, 58, 59, 60, 61, 62, where the discrete symmetries of graphene were discussed.

One can obtain from Eq. (8) the total electric current

$$\begin{aligned}\sum_{\mathbf{n}} j_\alpha(\mathbf{n}) &= e \int_{BZ} \frac{d^2\mathbf{k}}{(2\pi)^2} \sum_{\delta_i, \sigma} \Upsilon_\sigma^\dagger(\mathbf{k}) \frac{\partial}{\partial k_\alpha} \frac{t}{\hbar} \begin{pmatrix} 0 & e^{i\mathbf{k}\delta_i} \\ e^{-i\mathbf{k}\delta_i} & 0 \end{pmatrix} \Upsilon_\sigma(\mathbf{k}) \\ &\simeq -ev_F \sum_{\sigma} \int_{DC} \frac{d^2p}{(2\pi)^2} \bar{\Psi}_\sigma(\mathbf{p}) \gamma^\alpha \Psi_\sigma(\mathbf{p}),\end{aligned}\quad (53)$$

where in the second line, we expanded the matrix near the \mathbf{K}_\pm points and introduced 4-component spinors $\Psi_\sigma(\mathbf{p})$ and $\bar{\Psi}_\sigma(\mathbf{p})$. One can recognize that the form of the electric current operator and its coupling to the vector potential \mathbf{A} in Eq. (8) is standard for QED. Another famous condensed matter system, a d -wave superconductor, is also described (see e.g. Refs. 63, 64, 65, 66, 67, 68) in terms of QED $_{2+1}$, but the coupling to the vector potential is different due to the presence of supercurrents.

Thus putting together the Hamiltonian, Eq. (49), and the interaction term $\mathbf{A}(\mathbf{n})\mathbf{j}(\mathbf{n})$ (see Eq. (6)), where current density $\mathbf{j}(\mathbf{n})$ corresponds to the current operator in Eq. (53), we arrive at the QED $_{2+1}$ Lagrangian

$$\mathcal{L} = \sum_{\sigma=\pm 1} \bar{\Psi}_\sigma(t, \mathbf{r}) [i\gamma^0(\hbar\partial_t - i\mu_\sigma) + i\hbar v_F \gamma^1 D_x + i\hbar v_F \gamma^2 D_y] \Psi_\sigma(t, \mathbf{r}) \quad (54)$$

with $D_\alpha = \partial_\alpha + ie/\hbar c A_\alpha$, $\alpha = x, y$ written in the coordinate representation. In what follows we consider the setup when the external constant magnetic field $\mathbf{B} = \nabla \times \mathbf{A}$ is applied perpendicular to the graphene plane along the positive z axis. The magnetic field also enters the Zeeman term included via μ_σ . When the field \mathbf{B} is not perpendicular to the plane, the total field still enter the Zeeman term, while the orbital term would depend on its perpendicular component.

The theoretical explanation of the basic experiments^{14,15} which proved that Dirac quasiparticles exist in graphene is grounded in the Dirac Lagrangian (54).

Although the low-energy quasiparticle excitations described by (54) are noninteracting, this Lagrangian captures the Dirac nature of the quasiparticles. Moreover, for magnetic fields below 10 T, there is no need to include the Zeeman term²⁶ and the orbital effect of the magnetic field is sufficient. Nevertheless, dc^{26,27} and ac²⁹ measurements in strong fields $B \gtrsim 10$ T already indicate that the interaction between quasiparticles in graphene plays an important role. From a theoretical point of view, the effect of the long range Coulomb interaction had become a research topic long before the discovery of graphene.^{6,7,8,9} The Coulomb interaction Hamiltonian is

$$H_C = \frac{\hbar v_F}{2} \sum_{\sigma, \sigma'} \int d^2\mathbf{r} d^2\mathbf{r}' \bar{\Psi}_\sigma(\mathbf{r}) \gamma^0 \Psi_\sigma(\mathbf{r}) \frac{g}{|\mathbf{r} - \mathbf{r}'|} \bar{\Psi}_{\sigma'}(\mathbf{r}') \gamma^0 \Psi_{\sigma'}(\mathbf{r}'). \quad (55)$$

The coupling constant is $g = e^2/\epsilon\hbar v_F = \alpha c/\epsilon v_F$, where $\alpha \simeq 1/137$ is the fine-structure constant. With air on one side of the graphene plane and SiO₂ on the other, the unscreened dielectric constant of the medium is estimated in Ref. 69 to be $\epsilon \approx 1.6\epsilon_0$. The corresponding value of $g \approx 1.37$ is well above a simplifying assumption for theoretical analysis $g \ll 1$ and this explains why the effect of Coulomb interaction in graphene is a hot topic of ongoing research (see e.g. Refs. 70, 71, 72).

Besides long range Coulomb interaction, one can also consider other lattice interactions like on-site repulsion and nearest neighbor repulsion^{69,56}

$$\begin{aligned} H_{int} &= \frac{U}{2} \sum_{\mathbf{n}, \sigma, \sigma'} \Upsilon_\sigma^\dagger(\mathbf{n}) P_+ \Upsilon_\sigma(\mathbf{n}) \Upsilon_{\sigma'}^\dagger P_+(\mathbf{n}) \Upsilon_{\sigma'}(\mathbf{n}) \\ &+ \frac{U}{2} \sum_{\mathbf{n}, \sigma, \sigma'} \Upsilon_\sigma^\dagger(\mathbf{n} + \boldsymbol{\delta}_1) P_- \Upsilon_\sigma(\mathbf{n} + \boldsymbol{\delta}_1) \Upsilon_{\sigma'}^\dagger(\mathbf{n} + \boldsymbol{\delta}_1) P_- \Upsilon_{\sigma'}(\mathbf{n} + \boldsymbol{\delta}_1) \\ &+ \frac{V}{2} \sum_{\mathbf{n}, \boldsymbol{\delta}_i, \sigma, \sigma'} \Upsilon_\sigma^\dagger(\mathbf{n}) P_+ \Upsilon_\sigma(\mathbf{n}) \Upsilon_{\sigma'}^\dagger(\mathbf{n} + \boldsymbol{\delta}_i) P_- \Upsilon_{\sigma'}(\mathbf{n} + \boldsymbol{\delta}_i) \end{aligned} \quad (56)$$

with $P_\pm = (1 \pm \tau_3)/2$. In the low-energy continuum limit, this leads to several local four-fermion interaction terms,^{69,56} which in general break initial $U(4)$ invariance and the generation of corresponding gaps (see, Sec. 3.6):

$$H_{int} = \sum_i U_i \int d^2\mathbf{r} (\bar{\Psi}(\mathbf{r}) \Gamma_i \Psi(\mathbf{r}))^2, \quad \Gamma_i = (I, \gamma^3, \gamma^5, \gamma^3 \gamma^5) \otimes (\sigma_0, \sigma_3). \quad (57)$$

In summary, we would like to emphasize that the statement that the effective low-energy theory of graphene is massless QED₂₊₁ is based on three nontrivial facts:

- (i) Low-energy excitations in graphene are massless quasiparticles with linear dispersion which have positive and negative branches, $\pm \hbar v_F |\mathbf{p}|$. It is often underemphasized, that even the massive quasiparticles (see Sec. 3.6 and Fig. 3 (b) below) with the energy $\pm \sqrt{\hbar^2 v_F^2 \mathbf{p}^2 + \Delta^2}$ are still governed by the massive QED₂₊₁ rather than Schrödinger theory.
- (ii) A qualitatively new feature of graphene is that the eigenfunctions of the low energy quasiparticle excitations obey the Dirac equation. As we have seen, the

spinor structure of the wave functions is a general consequence of the honeycomb lattice structure of graphene with two carbon atoms per unit cell.^{1,53}

- (iii) It is crucial that interaction of the quasiparticles in graphene with an external electromagnetic field be introduced using the minimal coupling prescription of quantum field theory.

3.3. Continuum symmetries of QED₂₊₁ model

In the absence of Zeeman splitting, $\mu_\sigma = \mu$ the effective Lagrangian (54) possesses global $U(4)$ symmetry which is discussed for example in Appendices A and C in Refs. 9, 55. This symmetry operates in the valley-sublattice and spin spaces. It is useful to ignore, for a moment, spin space and begin by considering a global $U(2)$ symmetry for the 4-component spinors in the valley-sublattice space.

3.3.1. $U(2)$ valley-sublattice symmetry

One can easily check that matrices

$$T_1 = \frac{1}{2}i\gamma^3 = \frac{1}{2}\tilde{\tau}_2 \otimes \tau_3, \quad T_2 = \frac{1}{2}\gamma^5 = \frac{1}{2}\tilde{\tau}_3 \otimes \tau_0, \quad T_3 = \frac{1}{2}\gamma^3\gamma^5 = \frac{1}{2}\tilde{\tau}_1 \otimes \tau_3 \quad (58)$$

commute with the Hamiltonian (44) and satisfy the commutation relations of $SU(2)$ algebra

$$[T_i, T_j] = i\epsilon_{ijk}T_k, \quad (59)$$

where ϵ_{ijk} is the Levi-Civita symbol. Together with the identity matrix ($T_0 = I_4/2$), they lead to the $U(2)$ symmetry^{73,9} which acts in the space of valley and sublattice indices. We will call this effective symmetry of the low-energy approximation for the lattice graphene Hamiltonian as chiral symmetry because it contains the γ^5 matrix and resembles chiral symmetries for massless particles in high energy physics (see a special Sec. 3.4 on chirality below). Because of chiral $SU(2)$ symmetry, there is a conserving quantum number chirality which is characterized by eigenvalues of a diagonal generator $T_2 = \gamma^5/2$. Since there are two eigenvalues $+1/2$ and $-1/2$ of the diagonal generator T_2 , the four-component spinor Ψ_σ is the reducible representation of the $SU(2)$ group. The conservation of chirality number plays an important role and leads to the absence of backscattering⁷⁴ in the presence of impurities that do not violate chiral symmetry.

We note that the matrix

$$S = \begin{pmatrix} 1 & 0 & 0 & 0 \\ 0 & 0 & 1 & 0 \\ 0 & 1 & 0 & 0 \\ 0 & 0 & 0 & -1 \end{pmatrix} = S^T = S^{-1} \quad (60)$$

brings the generators T_i to block-diagonal form

$$ST_1S^{-1} = \frac{1}{2} \begin{pmatrix} \tau_2 & 0 \\ 0 & \tau_2 \end{pmatrix}, \quad ST_2S^{-1} = \frac{1}{2} \begin{pmatrix} \tau_3 & 0 \\ 0 & \tau_3 \end{pmatrix}, \quad ST_3S^{-1} = \frac{1}{2} \begin{pmatrix} \tau_1 & 0 \\ 0 & \tau_1 \end{pmatrix}. \quad (61)$$

In this reducible representation, the spinor Ψ_σ acquires the form

$$\Psi_\sigma^S = S\Psi_\sigma = \begin{pmatrix} a_\sigma(\mathbf{K}_+ + \mathbf{p}) \\ b_\sigma(\mathbf{K}_- + \mathbf{p}) \\ b_\sigma(\mathbf{K}_+ + \mathbf{p}) \\ -a_\sigma(\mathbf{K}_- + \mathbf{p}) \end{pmatrix}, \quad (62)$$

where the two upper and two lower components correspond to the two irreducible representations of $SU(2)$ group.

3.3.2. $U(4)$ spin-valley-sublattice symmetry and its breaking by the Zeeman term

We now generalize the previous section and include rotations in spin space. The 16 generators of the $U(4)$ that operate in the spin and valley-sublattice space are

$$\frac{\sigma_\kappa}{2} \otimes I_4, \quad \frac{\sigma_\kappa}{2} \otimes i\gamma^3, \quad \frac{\sigma_\kappa}{2} \otimes \gamma^5, \quad \text{and} \quad \frac{\sigma_\kappa}{2} \otimes \frac{1}{2}[\gamma^3, \gamma^5], \quad (63)$$

where I_4 is the 4×4 unit matrix and σ_κ , with $\kappa = 0, 1, 2, 3$ being four Pauli matrices connected with spin degrees of freedom [σ_0 is the 2×2 unit matrix]. It is easy to see that when $B = 0$ and there is no Zeeman splitting, the Lagrangian (54) and the interaction term (55) are invariant under global $U(4)$ group generated by these 16 generators.

The simplest example of symmetry breaking is provided by the Zeeman term, $\Psi_\sigma^\dagger \sigma_3 \Psi = \bar{\Psi} \gamma^0 \sigma_3 \Psi$, where σ_3 acts on the spin indices σ of the Dirac spinors. It explicitly breaks the $U(4)$ down to the $U(2)_a \times U(2)_b$ with the generators

$$\frac{\sigma_{\kappa'}}{2} \otimes I_4, \quad \frac{\sigma_{\kappa'}}{2} \otimes i\gamma^3, \quad \frac{\sigma_{\kappa'}}{2} \otimes \gamma^5, \quad \text{and} \quad \frac{\sigma_{\kappa'}}{2} \otimes \frac{1}{2}[\gamma^3, \gamma^5], \quad (64)$$

where $\kappa' = 0, 3$. We will discuss other possible symmetry breaking terms in Sec. 3.6 below.

3.4. Chirality in QED₂₊₁ theory of graphene and its difference from the chirality in QED₃₊₁

Because in the massless Dirac theory γ^5 commutes with the Hamiltonian (44) (anticommutes with H_0^D given by (49)), it introduces the conserving *chirality* quantum number which corresponds to the valley index. Indeed the spinors

$$\Psi_{\mathbf{K}_+} = \begin{pmatrix} \psi_{\mathbf{K}_+} \\ 0 \end{pmatrix}, \quad \Psi_{\mathbf{K}_-} = \begin{pmatrix} 0 \\ \psi_{\mathbf{K}_-} \end{pmatrix} \quad (65)$$

that describe the quasiparticle excitations at \mathbf{K}_\pm points, respectively, are the eigenstates of γ^5 :

$$\gamma^5 \Psi_{\mathbf{K}_+} = \Psi_{\mathbf{K}_+}, \quad \gamma^5 \Psi_{\mathbf{K}_-} = -\Psi_{\mathbf{K}_-}. \quad (66)$$

The labeling of \mathbf{K}_\pm points by eigenstates of the chiral operator γ^5 is an advantage of the chiral representation (47) of the γ matrices. This is not the case in the often used basis (52) with diagonal γ^0 .

For massless particles in 3 + 1 dimensions, the chirality quantum number corresponds to the *helicity* which characterizes the projection of its spin on the direction of momentum. In the 2 + 1 dimensional case, the usual helicity concept for massless particles is meaningless and one may only talk about pseudohelicity.

Let us now illustrate this by considering the Dirac equation which follows from the Lagrangian (54) in the simplest $B = \mu = 0$ case, also dropping the spin index. We consider its positive and negative energy solutions with a definite chirality

$$\Psi_{\mathbf{K}_\pm}^e(t, \mathbf{r}) = e^{-i\frac{Et}{\hbar} + i\mathbf{r}\mathbf{p}} U_{\mathbf{K}_\pm}^e(E, \mathbf{p}), \quad \Psi_{\mathbf{K}_\pm}^h(t, \mathbf{r}) = e^{i\frac{Et}{\hbar} + i\mathbf{r}\mathbf{p}} U_{\mathbf{K}_\pm}^h(E, \mathbf{p}) \quad (67)$$

with $E = \hbar v_F |\mathbf{p}|$ which correspond to the electrons and holes from \mathbf{K}_\pm valleys, respectively. Substituting (67) in the Dirac equation, we obtain that the spinors

$$U_{\mathbf{K}_+}^{e,h}(E, \mathbf{p}) = \begin{pmatrix} \psi_{\mathbf{K}_+}^{e,h}(E, \mathbf{p}) \\ 0 \end{pmatrix}, \quad U_{\mathbf{K}_-}^{e,h}(E, \mathbf{p}) = \begin{pmatrix} 0 \\ \psi_{\mathbf{K}_-}^{e,h}(E, \mathbf{p}) \end{pmatrix} \quad (68)$$

satisfy Weyl equations, $\mathcal{H}_0(\mathbf{p})U^{e,h}(\mathbf{p}) = \pm EU^{e,h}(\mathbf{p})$ or for 2-component spinors,

$$\begin{aligned} \hbar v_F(\tau_1 p_1 + \tau_2 p_2)\psi_{\mathbf{K}_+}^{e,h} &= \pm E\psi_{\mathbf{K}_+}^{e,h}, \\ -\hbar v_F(\tau_1 p_1 + \tau_2 p_2)\psi_{\mathbf{K}_-}^{e,h} &= \pm E\psi_{\mathbf{K}_-}^{e,h}, \end{aligned} \quad (69)$$

where the upper sign corresponds to the electrons and lower to the holes, respectively. We stress that in our case the vector $\mathbf{p} = (p_1, p_2)$ is in the graphene plane. Formally, Eqs. (69) look similar to the Dirac-Weyl equations that describe massless neutrinos,⁷⁵

$$\hbar c\mathbf{p}\boldsymbol{\alpha}\Psi = \hbar c \begin{pmatrix} \mathbf{p}\boldsymbol{\sigma} & 0 \\ 0 & -\mathbf{p}\boldsymbol{\sigma} \end{pmatrix} \Psi = p_0\Psi, \quad (70)$$

but in the latter case, the space is 3D. This allows one to introduce, for a massless particle in 3 + 1 dimension, the *helicity* operator

$$\Lambda = \frac{\mathbf{p}\boldsymbol{\Sigma}}{|\mathbf{p}|}, \quad \boldsymbol{\Sigma} = \begin{pmatrix} \boldsymbol{\sigma} & 0 \\ 0 & \boldsymbol{\sigma} \end{pmatrix} \quad (71)$$

which commutes with the Dirac Hamiltonian $\hbar c\mathbf{p}\boldsymbol{\alpha}$ and characterizes the projection of particle spin on the direction of its momentum. Multiplying Eq. (70) by γ^5 and taking into account that massless particles (antiparticles) have the dispersion $p_0 = \pm\hbar c|\mathbf{p}|$, one obtains that $\gamma^5\Psi = \pm\mathbf{p}\boldsymbol{\Sigma}/|\mathbf{p}|\Psi$. This illustrates that, for massless particles, the helicity coincides with the chirality, while for antiparticles it has the opposite sign to the chirality.

Let us consider the solutions of Eq. (69) for the \mathbf{K}_+ point

$$\psi_{\mathbf{K}_+}^e(E, \mathbf{p}) = \frac{1}{\sqrt{2}} \begin{pmatrix} 1 \\ \frac{p_x + ip_y}{|\mathbf{p}|} \end{pmatrix}, \quad \psi_{\mathbf{K}_+}^h(E, \mathbf{p}) = \frac{1}{\sqrt{2}} \begin{pmatrix} \frac{-p_x + ip_y}{|\mathbf{p}|} \\ 1 \end{pmatrix}, \quad (72)$$

and \mathbf{K}_- point

$$\psi_{\mathbf{K}_-}^e(E, \mathbf{p}) = \frac{1}{\sqrt{2}} \begin{pmatrix} 1 \\ -\frac{p_x + ip_y}{|\mathbf{p}|} \end{pmatrix}, \quad \psi_{\mathbf{K}_-}^h(E, \mathbf{p}) = \frac{1}{\sqrt{2}} \begin{pmatrix} \frac{p_x - ip_y}{|\mathbf{p}|} \\ 1 \end{pmatrix}. \quad (73)$$

The 4-component spinors (65) made from the solutions (72), (73) are mutually orthogonal eigenstates of the Hamiltonian $\mathcal{H}_0(\mathbf{p})$ and the operator γ^5 :

$$\Psi_r^{i*}(\mathbf{p})\Psi_s^j(\mathbf{p}) = \delta^{ij}\delta_{rs}, \quad i, j = e, h, \quad r, s = \mathbf{K}_+, \mathbf{K}_-. \quad (74)$$

In the $2 + 1$ dimensional case one cannot make rotations around the direction of the quasiparticle momentum \mathbf{p} lying in the 2D plane and the operator $\boldsymbol{\tau} = (\tau_1, \tau_2)$ does not have the physical meaning of the usual spin operator. Therefore the concept of the helicity for massless particles related to the Lorentz group and the real space rotations is meaningless in this case.⁷⁶ Furthermore, since there is only one generator of angular momentum τ_3 , there is no non-abelian Lie algebra that can restrict its possible eigenvalues, giving rise to the possibility of exotic statistics (see Ref. 77 and references therein). The solutions (72) and (73) are double-valued under the rotations $R(\theta) = \exp(i\theta\tau_3/2)$ with $0 < \theta < 4\pi$, because they describe spinor fields.⁷⁶

Formally one can consider the pseudohelicity operator

$$\Lambda^{2D} = \frac{\mathbf{p}\boldsymbol{\Sigma}}{|\mathbf{p}|}, \quad \boldsymbol{\Sigma} = \begin{pmatrix} \boldsymbol{\tau} & 0 \\ 0 & \boldsymbol{\tau} \end{pmatrix}, \quad \boldsymbol{\tau} = (\tau_1, \tau_2) \quad (75)$$

which commutes with the Hamiltonian and thus corresponds to a conserving quantum number. This operator, however, would correspond to an internal symmetry rather than to spatial symmetry as in the $3 + 1$ dimensional case. Still one can relate chirality and pseudohelicity operators for massless quasiparticles, $\gamma^5\Psi = \pm\Lambda^{2D}\Psi$.

One can also see that the solutions in Eq. (72) and Eq. (73) which obey Eq. (74) differ only by the sign of momentum. Thus we arrive at the conclusion^{78,60,59} that at the \mathbf{K}_+ point, electronic excitations have energy $\hbar v_F|\mathbf{p}|$ and $\mathbf{p}\boldsymbol{\tau}/|\mathbf{p}|\psi_{\mathbf{K}_+}^e = \psi_{\mathbf{K}_+}^e$, while for holes the energy is $-\hbar v_F|\mathbf{p}|$, i.e. $\mathbf{p}\boldsymbol{\tau}/|\mathbf{p}|\psi_{\mathbf{K}_+}^h = -\psi_{\mathbf{K}_+}^h$. For the \mathbf{K}_- point, these relations are inverted: for electrons, $\mathbf{p}\boldsymbol{\tau}/|\mathbf{p}|\psi_{\mathbf{K}_-}^e = -\psi_{\mathbf{K}_-}^e$ and for holes, $\mathbf{p}\boldsymbol{\tau}/|\mathbf{p}|\psi_{\mathbf{K}_-}^h = \psi_{\mathbf{K}_-}^h$. For 4-component spinors $\Psi_{\mathbf{K}_\pm}^{e,h}$ these conditions can be rewritten using the pseudohelicity operator: $\Lambda^{2D}\Psi_{\mathbf{K}_\pm}^e = \pm\Psi_{\mathbf{K}_\pm}^e$ and $\Lambda^{2D}\Psi_{\mathbf{K}_\pm}^h = \mp\Psi_{\mathbf{K}_\pm}^h$. They imply that at any given \mathbf{K}_\pm point, the direction of the momentum for electrons and holes with the same absolute value of the energy is opposite. This property of the massless electrons and holes is the consequence of equations of motion. However, to forbid backscattering of the quasiparticles⁷⁴ one should also suppress the transfer of quasiparticles from one valley to another. This restriction is already associated with chirality conservation. For example, chirality is a good quantum number in a monolayer with electrostatic potential scattering.

We were able to define the chiral matrix γ^5 and the chirality quantum number, because we used the reducible 4×4 representation of the Dirac matrices. In $2 + 1$

20 V.P. GUSYNIN, S.G. SHARAPOV, J.P. CARBOTTE

dimensions, there are two inequivalent irreducible 2×2 representations of the Dirac algebra.⁷⁹ The corresponding 2×2 $\tilde{\gamma}$ matrices are characterized by their signature⁸⁰

$$\eta = \frac{i}{2} \text{Tr}[\tilde{\gamma}^0 \tilde{\gamma}^1 \tilde{\gamma}^2]. \quad (76)$$

One can check that $\hat{\gamma}^\nu$ and $\tilde{\gamma}^\nu$ matrices that constitute the 4×4 representation (52) have the opposite signatures $\eta = +1$ and $\eta = -1$, respectively. It turns out that taking into account two inequivalent \mathbf{K}_\pm points demands using two unitary inequivalent representations of 2×2 gamma matrices. As we saw in the chiral representation of 4×4 γ matrices, the \mathbf{K}_\pm points are distinguished by the chirality (valley) quantum number. The signature η of the corresponding 2×2 γ matrices is sometimes known as “chirality”.⁸⁰ We note that by itself, this sign is not observable and one should introduce either the Dirac mass or/and the magnetic field and consider their relative signs (see Sec. 3.6 below).

Finally, we note that in accordance with Eq. (33) the matrix α^3 anticommutes with the Hamiltonian (44): $\{\alpha^3, H_0\} = 0$. The consequence of this is that the spectrum of the Hamiltonian is symmetric with respect to the eigenvalue $E = 0$. The identity $\alpha^2 H_0^*(\mathbf{k}) \alpha^2 = -H_0(\mathbf{k})$ corresponds to Eq. (34) and guarantees the symmetry of the spectrum with respect to $E = 0$ even in the presence of a finite Dirac mass $\bar{\Psi} \gamma^3 \Psi$. Also the matrix γ^0 anticommutes with the Hamiltonians (44) and (49): $\{\gamma^0, H_0\} = \{\gamma^0, H_0^D\} = 0$. In Refs. 46, 50 the property of anticommutativeness of H_0 with α^3 matrix was called chiral symmetry, due to its analogy with anticommutativeness of γ^5 with the Dirac Lagrangian in $3 + 1$ dimensional case.^{81,82} Also sometimes the sign of the energy, $\varepsilon = \lambda v_F |\mathbf{k}|$, where $\lambda = 1$ corresponds to the conduction band and $\lambda = -1$ corresponds to the valence band is called the “chirality label”. We, however, keep the use of the word “chiral” for the characteristics which really involve the γ^5 matrix.

3.5. Discrete symmetries of QED₂₊₁ model of graphene

In the continuum description, the definitions of the discrete symmetry operations are not unique. In field theoretical studies of QED₂₊₁, there is a certain convention on (see e.g. Refs. 12, 79) how to define these operations. It is based on the assertion that the parity transformation corresponds to inverting only one axis, say x axis: $\mathcal{P}(x, y) \rightarrow (-x, y)$, because inverting both would be a rotation. Bearing in mind the condensed matter roots of the effective QED₂₊₁ model, the discrete symmetry operations introduced here are in accord with the operations defined in Sec. 2.3 for the tight-binding model. Knowledge of these symmetries allows us to properly classify possible symmetry breaking terms, avoiding the trap vividly described in Ref. 83.

3.5.1. The spatial inversion \mathcal{P}

As discussed in Sec. 2.3.1 spatial inversion should invert both axes and exchange both A and B atoms and \mathbf{K}_\pm points. Thus applying the definition (20) and (21) for

the 4-component spinor $\Psi_\sigma(\mathbf{p})$ given by Eq. (43), we define^b

$$\Psi_\sigma(\mathbf{p}) \longrightarrow \mathcal{P}\Psi_\sigma(\mathbf{p})\mathcal{P}^{-1} = P\Psi_\sigma(-\mathbf{p}), \quad P = \tilde{\tau}_1 \otimes \tau_0 = \gamma^0, \quad P^2 = 1. \quad (77)$$

Note that this operation of inversion of two spatial coordinates is not equivalent to a rotation through an angle π in the plane which is given by $\Psi(k_x, k_y) \rightarrow \exp(i\pi(i\gamma^1\gamma^2/2))\Psi(-k_x, -k_y)$ with $i\gamma^1\gamma^2/2$ being the generator of the corresponding rotation.

The invariance (22) of H_0 under \mathcal{P} now follows from the condition

$$P\mathcal{H}_0^D(\mathbf{p})P = \mathcal{H}_0^D(-\mathbf{p}) \quad (78)$$

on the Dirac Hamiltonian density (49). Eq. (78) generalizes the condition (23) on the 2×2 Hamiltonian density. It is easy to see that under this \mathcal{P} transformation, the current $\bar{\Psi}\sigma_0\gamma^\mu\Psi$ from Eq. (53) transforms as follows

$$\bar{\Psi}\sigma_0\gamma^0\Psi \xrightarrow{\mathcal{P}} \bar{\Psi}\sigma_0\gamma^0\Psi, \quad \bar{\Psi}\sigma_0\gamma^1\Psi \xrightarrow{\mathcal{P}} -\bar{\Psi}\sigma_0\gamma^1\Psi, \quad \bar{\Psi}\sigma_0\gamma^2\Psi \xrightarrow{\mathcal{P}} -\bar{\Psi}\sigma_0\gamma^2\Psi, \quad (79)$$

where the unit matrix σ_0 acts on the spin indices σ of the Dirac spinors. The interaction with fixed external magnetic field $eA_\alpha\bar{\Psi}\sigma_0\gamma^\alpha\Psi$ is invariant under spatial inversion.

3.5.2. Time reversal \mathcal{T}

The time reversal operator, (29) interchanges \mathbf{K}_\pm points but not sublattices. Accordingly when we define the action \mathcal{T} on the 4-component spinors $\Psi_\sigma(\mathbf{p})$, the part acting on the sublattice degree of freedom is^{60,59} τ_1 ^c

$$\Psi(\mathbf{p}) \longrightarrow \mathcal{T}\Psi(\mathbf{p})\mathcal{T}^{-1} = i\sigma_2 T\Psi(-\mathbf{p}), \quad T = \tilde{\tau}_1 \otimes \tau_1 = \gamma^1\gamma^5, \quad T^2 = 1, \quad (80)$$

where σ_2 acts on the spin indices of the spinor $\Psi_\sigma(\mathbf{p})$. Double \mathcal{T} -transformation gives $\mathcal{T}^2\Psi(\mathbf{p})\mathcal{T}^{-2} = -\Psi(\mathbf{p})$. Hence for time-reversal symmetric systems with odd number of fermions, the degeneracy of levels cannot be less than 2 (Kramers' degeneracy theorem). It is easy to see that \mathbf{K}_\pm points are indeed related by time-reversal symmetry

$$\Psi(\mathbf{p}) = \begin{pmatrix} a(\mathbf{K}_+ + \mathbf{p}) \\ b(\mathbf{K}_+ + \mathbf{p}) \\ b(\mathbf{K}_- + \mathbf{p}) \\ a(\mathbf{K}_- + \mathbf{p}) \end{pmatrix} \xrightarrow{\mathcal{T}} T\Psi(-\mathbf{p}) = \begin{pmatrix} a(\mathbf{K}_- - \mathbf{p}) \\ b(\mathbf{K}_- - \mathbf{p}) \\ b(\mathbf{K}_+ - \mathbf{p}) \\ a(\mathbf{K}_+ - \mathbf{p}) \end{pmatrix}, \quad (81)$$

where for simplicity, we ignored spin degrees of freedom.

^bThe $\psi_{\mathbf{K}_\pm}$ components of the spinor (43) are exchanged by the inversion and because the sublattices are already exchanged by the definition of $\psi_{\mathbf{K}_-}$, we have τ_0 acting in the sublattice space instead of τ_1 used in Eq. (21). This definition of \mathcal{P} coincides with the corresponding operator in the second paper in Ref. 59.

^cCompare with the definition of \mathcal{P} above which includes τ_0 .

22 *V.P. GUSYNIN, S.G. SHARAPOV, J.P. CARBOTTE*

In the time-coordinate representation, the transformation (80) and the corresponding transformations for the Dirac conjugated spinor are

$$\begin{aligned}\Psi(t, \mathbf{r}) &\rightarrow \mathcal{T}\Psi(t, \mathbf{r})\mathcal{T}^{-1} = i\sigma_2 T\Psi(-t, \mathbf{r}), \\ \bar{\Psi}(t, \mathbf{r}) &\rightarrow (\mathcal{T}\Psi(t, \mathbf{r})\mathcal{T}^{-1})^\dagger(\gamma^0)^* = -\bar{\Psi}(-t, \mathbf{r})i\sigma_2 T.\end{aligned}\quad (82)$$

The invariance (30) of H_0 under \mathcal{T} now follows from the condition

$$T\mathcal{H}_0^{D*}(\mathbf{p})T = \mathcal{H}_0^D(-\mathbf{p}).\quad (83)$$

on the Dirac Hamiltonian density (49). Eq. (83) generalizes the condition (31) on the 2×2 Hamiltonian density.

It is easy to see that under this \mathcal{T} transformation, the current $\bar{\Psi}\sigma_0\gamma^\mu\Psi$ from Eq. (53) transforms as follows

$$\bar{\Psi}\sigma_0\gamma^0\Psi \xrightarrow{\mathcal{T}} \bar{\Psi}\sigma_0\gamma^0\Psi, \quad \bar{\Psi}\sigma_0\gamma^1\Psi \xrightarrow{\mathcal{T}} -\bar{\Psi}\sigma_0\gamma^1\Psi, \quad \bar{\Psi}\sigma_0\gamma^2\Psi \xrightarrow{\mathcal{T}} -\bar{\Psi}\sigma_0\gamma^2\Psi.\quad (84)$$

When the external magnetic field is held fixed, the corresponding interaction term $\bar{\Psi}\sigma_0\gamma^\alpha\Psi$ now breaks the time-reversal symmetry.

3.5.3. Charge conjugation \mathcal{C}

The charge conjugation \mathcal{C} acquires nontrivial meaning when we consider the second quantized Dirac theory and introduce a transformation that exchanges particles and antiparticles (electrons and holes), leaving their spin and momentum unchanged.

Accordingly we define the action of \mathcal{C} on 4-component spinors $\Psi_\sigma(\mathbf{p})$:

$$\Psi_\sigma(\mathbf{p}) \longrightarrow \mathcal{C}\Psi_\sigma(\mathbf{p})\mathcal{C}^{-1} = C\bar{\Psi}_\sigma^T(\mathbf{p}), \quad C = \gamma^1, \quad (85)$$

where T denotes the transpose. The matrix C satisfies the identities^d

$$C = -C^{-1} = -C^\dagger = -C^T, \quad C(\gamma^\mu)^T C^{-1} = -\gamma^\mu, \quad \mu = 0, 1, 2. \quad (86)$$

It is easy to see that \mathcal{C} exchanges A and B sublattices

$$\Psi_\sigma(\mathbf{p}) = \begin{pmatrix} a_\sigma(\mathbf{K}_+ + \mathbf{p}) \\ b_\sigma(\mathbf{K}_+ + \mathbf{p}) \\ b_\sigma(\mathbf{K}_- + \mathbf{p}) \\ a_\sigma(\mathbf{K}_- + \mathbf{p}) \end{pmatrix} \xrightarrow{\mathcal{C}} \gamma^1\gamma^0\Psi_\sigma^{\dagger T}(\mathbf{p}) = \begin{pmatrix} -b_\sigma^\dagger(\mathbf{K}_+ + \mathbf{p}) \\ -a_\sigma^\dagger(\mathbf{K}_+ + \mathbf{p}) \\ a_\sigma^\dagger(\mathbf{K}_- + \mathbf{p}) \\ b_\sigma^\dagger(\mathbf{K}_- + \mathbf{p}) \end{pmatrix}. \quad (87)$$

For the Dirac conjugated spinor we find

$$\bar{\Psi}_\sigma(\mathbf{p}) \rightarrow \mathcal{C}\Psi_\sigma^\dagger(\mathbf{p})\mathcal{C}^{-1}\gamma^0 = (\gamma^1\gamma^0\Psi_\sigma(\mathbf{p}))^T\gamma^0 = (-\gamma^1\Psi_\sigma(\mathbf{p}))^T. \quad (88)$$

It is easy to see that under \mathcal{C} transformation, the current $\bar{\Psi}\sigma_0\gamma^\mu\Psi$ from Eq. (53) transforms as follows

$$\bar{\Psi}\sigma_0\gamma^\mu\Psi \xrightarrow{\mathcal{C}} -\bar{\Psi}\sigma_0\gamma^\mu\Psi, \quad \mu = 0, 1, 2. \quad (89)$$

One can also check that the Lagrangian (54) is invariant under \mathcal{C} if one simultaneously replaces $e \rightarrow -e$.

^dNotice that our definition of $C = \gamma^1$ coincides with Ref. 12 and that $C(\gamma^3)^T C^{-1} = \gamma^3$.

3.5.4. *Difference between quasiparticles in graphene and massless neutrinos*

There is a widespread analogy between quasiparticles in graphene and massless neutrinos which is based on the similarity of the Dirac-Weyl equations (70) and Eqs. (69) for quasiparticles in graphene.³⁷ Our consideration of the discrete \mathcal{P} , \mathcal{T} and \mathcal{C} symmetries in Secs. 3.5.1, 3.5.2 and 3.5.3 shows that this analogy is not complete. The Dirac equation (70) corresponds to a pair of Weyl equations for 2-component left-handed, $\Psi_L = (1/2)(1 - \gamma^5)\Psi$ and right-handed spinors $\Psi_R = (1/2)(1 + \gamma^5)\Psi$. These two equations are related to each other by parity transformation. It is assumed in particle physics that in nature, there exist only left-handed neutrinos, so that it is sufficient to use one Weyl equation. However, this single equation breaks \mathcal{C} and \mathcal{P} symmetries, but preserves \mathcal{CP} and \mathcal{T} symmetries.⁷⁵ The Dirac quasiparticles in graphene with a definite chirality are also described by one of the Weyl equations (69) for the 2-component spinor. The last equation, however, breaks \mathcal{P} and \mathcal{T} symmetries, but preserves \mathcal{PT} and \mathcal{C} symmetries. This conclusion about the difference of the discrete symmetries in QED₃₊₁ and graphene could not be made by a formal comparison of Eqs. (70) and (69), because one has to project the discrete symmetries of the lattice model from Sec. 2.3 into the continuum description of graphene. We also note that the fact that the \mathbf{K}_\pm points are related by time-reversal symmetry (see Eq. (81)) and this has an important implication for the Josephson effect in mesoscopic junctions consisting of a graphene layer contacted by two closely spaced superconducting electrodes.⁸⁴ As Cooper pairs are made up of time reversed electron states, the two electrons in Cooper pairs that are injected from the superconducting electrodes into graphene go to opposite \mathbf{K}_\pm points.⁸⁵ Finally, we note that the consideration of discrete symmetries allows one to make an analogy between the \mathbf{K}_\pm index and the circular polarization quantum number for photons. Indeed, photons with a definite circular polarization also break parity and time-reversal symmetries, but not charge conjugation.

3.6. *Dirac masses, their transformation under \mathcal{P} , \mathcal{T} , \mathcal{C} and physical meaning*

One of the main reason why graphene is attracting the attention of many theoreticians^{8,9,31,55,56,86,69,87,88,89,90,91,92,93} is that the electron-electron interactions and/or the magnetic field result in the breakdown of the $U(4)$ symmetry and in new physics whose understanding demands going beyond the unconventional yet rather simple physics of noninteracting Dirac quasiparticles.

For example, it is argued that the new zero filling factor state in the IQHE in graphene, seen in a strong magnetic field $B \gtrsim 20$ T is related to a spin polarized state^{26,27,28}, while $\nu = \pm 1$ states^{26,28} are related to the lifting of sublattice or valley degeneracy. The spin polarized state is described by the order parameter $\langle \bar{\Psi}\gamma^0\sigma_3\Psi \rangle$ (or more general $\langle \bar{\Psi}\gamma^0\sigma\Psi \rangle$) which makes it similar to the Zeeman term, but in contrast, it originates from many-body interactions.

Another channel of spontaneous breaking of the $U(4)$ symmetry down to $U(2)_c \times$

24 V.P. GUSYNIN, S.G. SHARAPOV, J.P. CARBOTTE

$U(2)_d$, is related to a possibility of the generation by the interactions of the Dirac mass M_D which enters the Lagrangian (54) in the following way

$$\mathcal{L} = \bar{\Psi}(t, \mathbf{r}) \left[i\gamma^0 \left(\hbar\sigma_0\partial_t - i\sigma_0\mu + i\sigma_3\frac{g}{2}\mu_B B \right) + i\hbar v_F\sigma_0\gamma^1 D_x + i\hbar v_F\sigma_0\gamma^2 D_y - M_D \right] \Psi(t, \mathbf{r}). \quad (90)$$

The Dirac mass M_D ^e has a general form $\Delta\sigma_\kappa \otimes \Gamma \equiv \Delta\sigma_\kappa\Gamma$, where Δ is its absolute value, σ_κ is one of the Pauli matrices (in what follows, we consider only σ_0 and σ_3 , more general masses with σ were recently considered in Ref. 92) and Γ is one of the four matrices

$$I_4, \quad \gamma^3, \quad i\gamma^5, \quad \gamma^3\gamma^5. \quad (91)$$

Under $SU(2)$ group (as in Sec. 3.3.1 we ignore for a moment the spin degree of freedom) the gaps $\bar{\Psi}\Psi$, $\bar{\Psi}\gamma^3\Psi$, $\bar{\Psi}i\gamma^5\Psi$ transform as a vector, while the gap $\bar{\Psi}\gamma^3\gamma^5\Psi$ is a scalar. Three gaps, $\bar{\Psi}\Psi$, $\bar{\Psi}\gamma^3\Psi$, and $\bar{\Psi}i\gamma^5\Psi$ break the $SU(2)$ group down to $U(1)$ subgroup (with generators T_3 , T_2 and T_1 being unbroken, respectively).

3.6.1. Physical meaning of the Dirac masses

To understand the physical meaning of one of the masses, let us rewrite the Hamiltonian H_1 defined by Eq. (24) in terms of 4-component spinor (43)

$$\begin{aligned} H_1 &= \sum_{\sigma} \int_{DC} \frac{d^2p}{(2\pi)^2} \Psi_{\sigma}^{\dagger}(\mathbf{p}) [m_+\tilde{\tau}_0 \otimes \tau_0 + m_-\tilde{\tau}_3 \otimes \tau_3] \Psi_{\sigma}(\mathbf{p}), \\ &= \int_{DC} \frac{d^2p}{(2\pi)^2} \bar{\Psi}(\mathbf{p}) [m_+\sigma_0\gamma^0 + m_-\sigma_0\gamma^3] \Psi(\mathbf{p}). \end{aligned} \quad (92)$$

As was already mentioned after Eq. (24), the term $m_+\sigma_0\gamma^0$ changes the total carrier density of both A and B sublattices and can thus be absorbed in the term with the chemical potential $\mu\sigma_0\gamma^0$. However, the term $m_-\sigma_0\gamma^3$ breaks \mathcal{P} defined by Eq. (77) and is an example of one of the Dirac masses introduced above. The operator

$$\begin{aligned} \int d^2x \bar{\Psi}\sigma_0\gamma^3\Psi &= \sum_{\sigma} \int_{DC} \frac{d^2p}{(2\pi)^2} [a_{\sigma}^{\dagger}(\mathbf{K}_+ + \mathbf{p})a_{\sigma}(\mathbf{K}_+ + \mathbf{p}) + a_{\sigma}^{\dagger}(\mathbf{K}_- + \mathbf{p})a_{\sigma}(\mathbf{K}_- + \mathbf{p}) \\ &\quad - b_{\sigma}^{\dagger}(\mathbf{K}_+ + \mathbf{p})b_{\sigma}(\mathbf{K}_+ + \mathbf{p}) - b_{\sigma}^{\dagger}(\mathbf{K}_- + \mathbf{p})b_{\sigma}(\mathbf{K}_- + \mathbf{p})] \end{aligned} \quad (93)$$

determines the magnitude of the order parameter $\langle \bar{\Psi}\sigma_0\gamma^3\Psi \rangle$ (and hence the fermion gap) proportional to the electron density imbalance between the A and B sublattices and corresponds to the formation of a site-centered charge density wave (CDW) in the excitonic insulating ground state⁸ which lifts sublattice degeneracy. As we have already mentioned in Sec. 2.3.1, it has been suggested⁴⁷ that this kind of Dirac mass can be introduced in graphene by placing it on top an appropriate substrate

^eThe energy gap M_D is expressed via the corresponding Dirac mass m as $M_D = mv_F^2$. In what follows we ignore a difference between ‘‘Dirac gap’’ and ‘‘Dirac mass’’ and use the term ‘‘Dirac mass’’ for both of them.

which breaks the graphene sublattice symmetry between A and B and so generates an intrinsic Dirac mass for the fermions.

The Dirac mass can also be generated dynamically. Historically the phenomenon of the electron-hole (fermion-antifermion) pairing in a magnetic field called *magnetic catalysis* was revealed in field theory.⁹⁴ Later, the experiments on graphite and their interpretation in terms of the Dirac fermions⁹⁵ inspired a theoretical condensed matter consideration of this kind of Dirac mass.^{8,9,96,54} Note that in the notations of these papers, it corresponds to $\bar{\Psi}\Psi$. In the present conventions, the term $\bar{\Psi}\Psi$ yields a chiral mixing between \mathbf{K}_{\pm} points:

$$\int d^2x \bar{\Psi} \sigma_0 \Psi = \sum_{\sigma} \int_{DC} \frac{d^2p}{(2\pi)^2} [a_{\sigma}^{\dagger}(\mathbf{K}_+ + \mathbf{p}) b_{\sigma}(\mathbf{K}_- + \mathbf{p}) + b_{\sigma}^{\dagger}(\mathbf{K}_+ + \mathbf{p}) a_{\sigma}(\mathbf{K}_- + \mathbf{p}) + b_{\sigma}^{\dagger}(\mathbf{K}_- + \mathbf{p}) a_{\sigma}(\mathbf{K}_+ + \mathbf{p}) + a_{\sigma}^{\dagger}(\mathbf{K}_- + \mathbf{p}) b_{\sigma}(\mathbf{K}_+ + \mathbf{p})] \quad (94)$$

This term preserves \mathcal{P} , \mathcal{T} and \mathcal{C} symmetries.

Magnetic catalysis is one of the candidates (see Ref. 31 for an overview of all scenarios) for an explanation of the new QHE states observed in graphene in high magnetic fields.^{26,27,28} In particular, Refs. 55, 56, 90, 91 are devoted to the further development of this scenario. The latest experimental results^{27,28,29} pose new questions that have to be addressed in the future theoretical work on spontaneous symmetry breaking and other competing models that attempt to explain the origin of $\nu = 0, \pm 1$ IQHE states. Here we will not go into the details of magnetic catalysis but instead consider all theoretically possible Dirac masses. Their physical meaning becomes clear when we write them in terms of the tight-binding model of graphene. Also we investigate their discrete symmetry properties.

Similarly to the mass in Eq. (94), the mass term with $\Gamma = \gamma^5$ also mixes \mathbf{K}_{\pm} points

$$\int d^2x \bar{\Psi} \sigma_0 i \gamma^5 \Psi = -i \sum_{\sigma} \int \frac{d^2p}{(2\pi)^2} [a_{\sigma}^{\dagger}(\mathbf{K}_+ + \mathbf{p}) b_{\sigma}(\mathbf{K}_- + \mathbf{p}) + b_{\sigma}^{\dagger}(\mathbf{K}_+ + \mathbf{p}) a_{\sigma}(\mathbf{K}_- + \mathbf{p}) - b_{\sigma}^{\dagger}(\mathbf{K}_- + \mathbf{p}) a_{\sigma}(\mathbf{K}_+ + \mathbf{p}) - a_{\sigma}^{\dagger}(\mathbf{K}_- + \mathbf{p}) b_{\sigma}(\mathbf{K}_+ + \mathbf{p})] \quad (95)$$

and breaks \mathcal{P} and \mathcal{C} symmetries. The order parameters in Eqs. (94) and (95) are related to a Kekulé distortion¹¹ which is $\text{Re}\Delta\bar{\Psi}\Psi - \text{Im}\Delta\bar{\Psi}i\gamma^5\Psi$ and breaks in general \mathcal{P} symmetry.

Another interesting example is the mass term with $\Gamma = \gamma^3\gamma^5$ for which one has

$$\int d^2x \bar{\Psi} \sigma_0 \gamma^3 \gamma^5 \Psi = \sum_{\sigma} \int \frac{d^2p}{(2\pi)^2} [a_{\sigma}^{\dagger}(\mathbf{K}_+ + \mathbf{p}) a_{\sigma}(\mathbf{K}_+ + \mathbf{p}) - a_{\sigma}^{\dagger}(\mathbf{K}_- + \mathbf{p}) a_{\sigma}(\mathbf{K}_- + \mathbf{p}) - b_{\sigma}^{\dagger}(\mathbf{K}_+ + \mathbf{p}) b_{\sigma}(\mathbf{K}_+ + \mathbf{p}) + b_{\sigma}^{\dagger}(\mathbf{K}_- + \mathbf{p}) b_{\sigma}(\mathbf{K}_- + \mathbf{p})]. \quad (96)$$

In contrast to the gap (mass) in Eq. 93), the gap in Eq. (96) corresponds to a gap with the opposite sign at \mathbf{K}_- point [cf. Eqs. (96) and (93)]. As pointed out in the second paper of Ref. 58 it is related to a model introduced by Haldane⁴ as a

26 *V.P. GUSYNIN, S.G. SHARAPOV, J.P. CARBOTTE*

realization of the parity anomaly in 2 + 1 dimensional field theory (see also Refs. 3, 5, 83). Notice another definition of the spinor

$$\Psi'_\sigma = (a_\sigma^\dagger(\mathbf{K}_+ + \mathbf{p}), b_\sigma^\dagger(\mathbf{K}_+ + \mathbf{p}), a_\sigma^\dagger(\mathbf{K}_- + \mathbf{p}), b_\sigma^\dagger(\mathbf{K}_- + \mathbf{p})) \quad (97)$$

in Ref. 58, so that the gap in Eq. (96) term becomes $\Psi'^\dagger \sigma_0 \otimes \tilde{\tau}_3 \otimes \tau_3 \Psi'$ ($\tilde{\tau}$ and τ matrices act in valley and sublattice spaces, respectively). In our conventions (43) this corresponds to $\Psi'^\dagger \sigma_0 \otimes \tilde{\tau}_0 \otimes \tau_3 \Psi = \bar{\Psi} \sigma_0 \gamma^3 \gamma^5 \Psi$ gap. Comparing the masses in Eqs. (93) and (96), one finds that the second mass preserves \mathcal{P} . On the other hand, considering that \mathbf{K}_\pm points are related by time-reversal \mathcal{T} (see Eq. (81)), one can easily see that while the mass term $\Delta \sigma_0 \gamma^3$ preserves \mathcal{T} , the mass $\Delta \tau \sigma_0 \gamma^3 \gamma^5$ breaks it. This is also illustrated by the the corresponding energies of the LLL given by Eqs. (101) and (106), respectively. In contrast, the mass $\sim \sigma_3 \gamma^3 \gamma^5$ which is related to the spin-orbit interaction⁵⁸ does not break \mathcal{T} . In fact, the gaps $\sigma_3 \gamma^3 \gamma^5$ and $\sigma_0 \otimes I_4$ are the only gaps that respect all the discrete symmetries.

Yet another option for the Dirac mass which involves spin degrees of freedom was recently considered in Ref. 56

$$\int d^2x \bar{\Psi} \sigma_3 \gamma^3 \Psi = \sum_\sigma \int \frac{d^2p}{(2\pi)^2} \sigma [a_\sigma^\dagger(\mathbf{K}_+ + \mathbf{p}) a_\sigma(\mathbf{K}_+ + \mathbf{p}) + a_\sigma^\dagger(\mathbf{K}_- + \mathbf{p}) a_\sigma(\mathbf{K}_- + \mathbf{p}) - b_\sigma^\dagger(\mathbf{K}_+ + \mathbf{p}) b_\sigma(\mathbf{K}_+ + \mathbf{p}) - b_\sigma^\dagger(\mathbf{K}_- + \mathbf{p}) b_\sigma(\mathbf{K}_- + \mathbf{p})]. \quad (98)$$

Since \mathcal{P} transformation does not affect the spin variable, this mass breaks this symmetry as does the mass (93). However, in contrast to this latest case, the mass (98) is also \mathcal{T} breaking.

All possible Dirac mass terms $\bar{\Psi} M_D \Psi$ and their transformation properties under \mathcal{P} , \mathcal{T} , \mathcal{C} symmetries are summarized in Table 1. For completeness we also included matrices M_μ , M_Z and $\mathcal{M}_{\mu 1}$, $\mathcal{M}_{\mu 2}$ that correspond to the chemical potential, Zeeman term and generalized chemical potentials, respectively. For convenience of comparison with Ref. 58 we provide equivalents M' of these terms for Ψ' and Ψ'^\dagger spinors (97).

Concerning the continuous $U(4)$ symmetry group, all Dirac gaps except $\sigma_0 \otimes \gamma^3 \gamma^5$ break it down to $U(2) \otimes U(2)$ subgroup though the pattern of breaking depends on a concrete gap. For example, in case of the gap $\Delta \bar{\Psi} \gamma^3 \Psi$ we have breakdown of $U(4)$ to the $U_a(2) \otimes U_b(2)$ with the generators

$$\frac{\sigma^a}{2} \otimes I_4, \quad \frac{\sigma^a}{2} \otimes T_2. \quad (99)$$

Subgroups $U_{a,b}(2)$ act in the state spaces (\mathbf{K}_+, \uparrow) , $(\mathbf{K}_+, \downarrow)$ and (\mathbf{K}_-, \uparrow) , $(\mathbf{K}_-, \downarrow)$, not mixing these two spaces.

An interesting example of $U(4)$ symmetry breaking is provided by the gap $\bar{\Psi} \sigma_3 \gamma^3 \Psi$. In this case, we have 8 unbroken generators

$$\frac{\sigma^1}{2} \otimes T_1, \quad \frac{\sigma^2}{2} \otimes T_1, \quad \frac{\sigma^1}{2} \otimes T_3, \quad \frac{\sigma^2}{2} \otimes T_3, \quad \frac{\sigma^0}{2} \otimes T_2, \quad \frac{\sigma^3}{2} \otimes T_2, \quad \frac{\sigma^0}{2} \otimes I_4, \quad \frac{\sigma^3}{2} \otimes I_4, \quad (100)$$

Table 1. Transformation properties of the various Dirac mass terms $\bar{\Psi}M_D\Psi = \Psi^\dagger M\Psi = \Psi'^\dagger M'\Psi'$ with $M_D = \sigma_{0,3} \otimes \Gamma$ under \mathcal{P} , \mathcal{T} and \mathcal{C} transformations. The matrices M_μ , M_Z and $\mathcal{M}_{\mu 1}, \mathcal{M}_{\mu 2}$ correspond to the chemical potential, Zeeman term and generalized chemical potentials, respectively.

| M_D | M | M' | \mathcal{P} | \mathcal{T} | \mathcal{C} |
|---|--|--|---------------|---------------|---------------|
| $\sigma_0 \otimes I_4$ | $\sigma_0 \otimes \tilde{\tau}_1 \otimes \tau_0$ | $\sigma_0 \otimes \tilde{\tau}_1 \otimes \tau_1$ | 1 | 1 | 1 |
| $\sigma_0 \otimes \gamma^3$ | $\sigma_0 \otimes \tilde{\tau}_3 \otimes \tau_3$ | $\sigma_0 \otimes \tilde{\tau}_0 \otimes \tau_3$ | -1 | 1 | 1 |
| $\sigma_0 \otimes i\gamma^5$ | $\sigma_0 \otimes \tilde{\tau}_2 \otimes \tau_0$ | $\sigma_0 \otimes \tilde{\tau}_2 \otimes \tau_1$ | -1 | 1 | -1 |
| $\sigma_0 \otimes \gamma^3\gamma^5$ | $\sigma_0 \otimes \tilde{\tau}_0 \otimes \tau_3$ | $\sigma_0 \otimes \tilde{\tau}_3 \otimes \tau_3$ | 1 | -1 | 1 |
| $\sigma_3 \otimes I_4$ | $\sigma_3 \otimes \tilde{\tau}_1 \otimes \tau_0$ | $\sigma_3 \otimes \tilde{\tau}_1 \otimes \tau_1$ | 1 | -1 | 1 |
| $\sigma_3 \otimes \gamma^3$ | $\sigma_3 \otimes \tilde{\tau}_3 \otimes \tau_3$ | $\sigma_3 \otimes \tilde{\tau}_0 \otimes \tau_3$ | -1 | -1 | 1 |
| $\sigma_3 \otimes i\gamma^5$ | $\sigma_3 \otimes \tilde{\tau}_2 \otimes \tau_0$ | $\sigma_3 \otimes \tilde{\tau}_2 \otimes \tau_1$ | -1 | -1 | -1 |
| $\sigma_3 \otimes \gamma^3\gamma^5$ | $\sigma_3 \otimes \tilde{\tau}_0 \otimes \tau_3$ | $\sigma_3 \otimes \tilde{\tau}_3 \otimes \tau_3$ | 1 | 1 | 1 |
| $M_\mu = \sigma_0 \otimes \gamma^0$ | $\sigma_0 \otimes \tilde{\tau}_0 \otimes \tau_0$ | $\sigma_0 \otimes \tilde{\tau}_0 \otimes \tau_0$ | 1 | 1 | -1 |
| $M_Z = \sigma_3 \otimes \gamma^0$ | $\sigma_3 \otimes \tilde{\tau}_0 \otimes \tau_0$ | $\sigma_3 \otimes \tilde{\tau}_0 \otimes \tau_0$ | 1 | -1 | -1 |
| $\mathcal{M}_{\mu 1} = \sigma_0 \otimes \gamma^0\gamma^5$ | $\sigma_0 \otimes -i\tilde{\tau}_2 \otimes \tau_0$ | $\sigma_0 \otimes -i\tilde{\tau}_2 \otimes \tau_1$ | -1 | -1 | -1 |
| $\mathcal{M}_{\mu 2} = \sigma_3 \otimes \gamma^0\gamma^5$ | $\sigma_3 \otimes -i\tilde{\tau}_2 \otimes \tau_0$ | $\sigma_3 \otimes -i\tilde{\tau}_2 \otimes \tau_1$ | -1 | 1 | -1 |

which form another $U_{a'}(2) \otimes U_{b'}(2)$ group acting in the state spaces (\mathbf{K}_+, \uparrow) , $(\mathbf{K}_-, \downarrow)$ and $(\mathbf{K}_+, \downarrow)$, (\mathbf{K}_-, \uparrow) , respectively. While this gap is \mathcal{P} -odd, \mathcal{T} -odd it is invariant under combined \mathcal{PT} -inversion.

Finishing our classification of the Dirac masses, we mention that the QED₂₊₁ description of d -wave superconductivity also involves various Dirac masses^{64,65,66,67,68} when the possible opening of a secondary gap is considered (for example, a charge or spin density wave or a second superconducting order parameter with different symmetry).

3.6.2. Dirac Landau levels

In an external magnetic field B Dirac Landau levels are formed. In the presence of a finite gap amplitude $\Delta \neq 0$ and ignoring the Zeeman splitting, for the matrices $\Gamma = I_4, \gamma^3, \gamma^5$ the energies of Landau levels are

$$E_n = \begin{cases} \pm \Delta \text{sgn}(eB), & n = 0, \\ \text{sgn}(n) \sqrt{\Delta^2 + 2|n|\hbar v_F^2|eB|/c}, & n = \pm 1, \pm 2, \dots \end{cases} \quad (101)$$

To understand how the spectrum (101) emerges, it is instructive to write the Dirac equation for one of these masses, considering separately each \mathbf{K} point. For example, for the $\Delta\sigma_0\gamma^3$ mass, one obtains

$$[i\tau_0\hbar\partial_t + i\hbar v_F\tau_1 D_x + i\hbar v_F\tau_2 D_y - \tau_3\Delta] \psi_{\mathbf{K}_+}(t, \mathbf{r}) = 0, \quad (102)$$

$$[i\tau_0\hbar\partial_t - i\hbar v_F\tau_1 D_x - i\hbar v_F\tau_2 D_y + \tau_3\Delta] \psi_{\mathbf{K}_-}(t, \mathbf{r}) = 0. \quad (103)$$

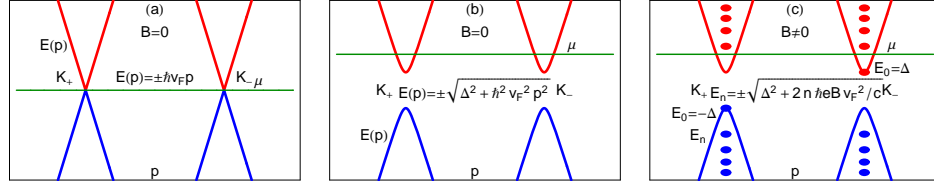
28 *V.P. GUSYNIN, S.G. SHARAPOV, J.P. CARBOTTE*


Fig. 3. (Colour online) Band structure of graphene. Electrons are shown in red and holes in blue. (a) The low-energy linear-dispersion $E(\mathbf{k})$ near the Dirac \mathbf{K}_+ and \mathbf{K}_- points for $B = 0$. (b) A possible modification of the quasiparticle spectrum by the finite gap (Dirac mass) Δ . The chemical potential (indicated by horizontal line) μ is shifted from zero by the gate voltage. (c) Landau levels E_n in the Dirac theory of graphene. Spin degree of freedom is ignored. For a given direction of the magnetic field \mathbf{B} applied perpendicular to graphene's plane, the lowest ($n = 0$) Landau level has the energy $E_0 = -\Delta$ at \mathbf{K}_+ and $E_0 = \Delta$ at \mathbf{K}_- .

Multiplying the left side of Eq. (102) by τ_3 and the left side of Eq. (103) by $-\tau_3$, one obtains

$$[i\hat{\gamma}^0 \hbar \partial_t + i\hbar v_F \hat{\gamma}^1 D_x + i\hbar v_F \hat{\gamma}^2 D_y - \Delta] \psi_{\mathbf{K}_+}(t, \mathbf{r}) = 0, \quad (104)$$

$$[i\hat{\gamma}^0 \hbar \partial_t + i\hbar v_F \hat{\gamma}^1 D_x + i\hbar v_F \hat{\gamma}^2 D_y - \Delta] \psi_{\mathbf{K}_-}(t, \mathbf{r}) = 0, \quad (105)$$

where in Eq. (104), 2×2 gamma matrices are given by Eq. (52) and in Eq. (105) $\tilde{\gamma}^0 = -\hat{\gamma}^0$, $\tilde{\gamma}^{1,2} = \hat{\gamma}^{1,2}$ and have the opposite signature η . For reference, the solution of Eqs. (104) and (105) in an external magnetic field is written down in Appendix A. The energies of the Landau levels with n and $-n$ for $|n| \geq 1$ are symmetric (see Eqs. (101) and (106)). The LLL is, however, asymmetric and anomalous, because for Eq. (104) its energy is $-\Delta \operatorname{sgn}(eB)$, while for Eq. (105), its energy is $\Delta \operatorname{sgn}(eB)$ (see Fig. 3 (c) where the case $eB > 0$ is shown). It turns out that the sign of the LLL energy is defined by the relative sign of the signature η of the 2×2 Dirac matrices (76) and the Dirac mass Δ .⁸⁰ This implies that because the sign before the mass Δ in Eqs. (104) and (105) is the same, the sign of the LLL energy depends on the sign of the signature of $\hat{\gamma}^\nu$ and $\tilde{\gamma}^\nu$ matrices. Thus altogether the combined energy spectrum of Eqs. (102) and (103) is symmetric and given by Eq. (101). This reflects the fact that the Dirac mass $\Delta \sigma_0 \gamma^3$ does not break the time-reversal symmetry.

In the limit $\Delta \rightarrow 0$, the Landau levels $\pm \Delta \operatorname{sgn}(eB)$ corresponding to $n = 0$ Landau levels merge together to form a single level. However, for $\mu = 0$ and ignoring Zeeman splitting, it remains half-filled. This property of the LLL equally shared by particles and antiparticles is at the heart of the unconventional QHE in graphene.¹⁷

For $\Gamma = \gamma^3 \gamma^5$, the spectrum is asymmetric

$$E_n = \begin{cases} -\Delta \operatorname{sgn}(eB), & n = 0, \\ \operatorname{sgn}(n) \sqrt{\Delta^2 + 2|n| \hbar v_F^2 |eB| / c}, & n = \pm 1, \pm 2, \dots \end{cases} \quad (106)$$

Indeed, the \mathcal{T} breaking $\Delta \mathcal{T} \sigma_0 \gamma^3 \gamma^5$ mass results in two equations

$$\begin{aligned} [i\tau_0 \hbar \partial_t + i\hbar v_F \tau_1 D_x + i\hbar v_F \tau_2 D_y - \tau_3 \Delta \mathcal{T}] \psi_{\mathbf{K}_+}(t, \mathbf{r}) &= 0, \\ [i\tau_0 \hbar \partial_t - i\hbar v_F \tau_1 D_x - i\hbar v_F \tau_2 D_y - \tau_3 \Delta \mathcal{T}] \psi_{\mathbf{K}_-}(t, \mathbf{r}) &= 0 \end{aligned} \quad (107)$$

which have the same sign before $\Delta_{\mathcal{T}}$. Accordingly, because the corresponding 2×2 gamma matrices are the same as for Eqs. (104) and (105), one can readily see that both equations in (107) lead to the same sign of the LLL energy, viz. $-\Delta_{\mathcal{T}} \text{sgn}(eB)$. Accordingly, the LLL remains doubly degenerate. Therefore, the combined energy spectrum (106) is obviously asymmetric. Thus, the time-reversal breaking character of the Dirac mass $\Delta_{\mathcal{T}}\sigma_0\gamma^3\gamma^5$ is revealed by an external magnetic field. At temperatures well below $\Delta_{\mathcal{T}}$ this leads to the QHE even in zero magnetic field.⁴ Indeed, since the transverse Hall conductivity σ_{xy} is odd under time reversal, a nonzero σ_{xy} can occur if time-reversal invariance is broken.

In the limit $\Delta_{\mathcal{T}} \rightarrow 0$, the $n = 0$ Landau level $-\Delta \text{sgn}(eB)$ in Eq. (106) is either electron-like or hole-like depending on the relative sign of Δ and eB . Thus, the generic zero gap limit is indefinite in terms of a clear particle or hole character of quasiparticles occupying the LLL. Nevertheless, from a physical point of view, the property of the LLL to be equally shared by particles and antiparticles can be argued by the presence of the Zeeman term.

The degeneracy of Landau levels with $n = \pm 1, \pm 2, \dots$ in Eqs. (101) and (106) is $|eB|/(\pi\hbar)$ (per unit area and per spin), while the degeneracy of the lowest Landau levels (LLL) $n = 0$ for Eq. (101) is $|eB|/(2\pi\hbar)$ and for Eq. (106) is $|eB|/(\pi\hbar)$.

It is worth emphasizing that it is the spectacular ‘‘relativistic’’ energy Landau scale $L(B) = \sqrt{|eB|\hbar v_F^2/c}$ which defines the distance between Landau levels

$$\Delta E = E_1(\Delta = 0) - E_0(\Delta = 0) = \sqrt{2L^2(B)} \approx 424\sqrt{B[\text{T}]} \text{K}. \quad (108)$$

For instance, it corresponds to $\Delta E \approx 2800 \text{ K}$ at $B = 45 \text{ T}$ which makes it possible for the QHE in graphene to be observed at room temperature.²⁰

Including the real spin degree of freedom, we have the following situation for Landau levels in a magnetic field with the \mathcal{P} -odd, \mathcal{T} -even gap $\Delta\bar{\Psi}\gamma^3\Psi$.^f For levels $n \geq 1$ all Landau levels are 4-fold degenerate (states $|\mathbf{K}_+, \uparrow\rangle, |\mathbf{K}_+, \downarrow\rangle, |\mathbf{K}_-, \uparrow\rangle, |\mathbf{K}_-, \downarrow\rangle$). On the other hand, for the $n = 0$ Landau levels, as shown in Fig. 4 (a), we have 2-fold degeneracy: states $|\mathbf{K}_+, \uparrow\rangle, |\mathbf{K}_+, \downarrow\rangle$ and $|\mathbf{K}_-, \uparrow\rangle, |\mathbf{K}_-, \downarrow\rangle$ with energies $\mp\Delta$, respectively. For \mathcal{P} -odd, \mathcal{T} -odd gap $\Delta\bar{\Psi}\sigma_3\gamma^3\Psi$ (see Fig. 4 (b)) the situation with levels $n \geq 1$ is the same, but two Landau levels with $n = 0$ with energies $\mp\Delta$ now have different 2-fold degeneracies: $|\mathbf{K}_+, \uparrow\rangle, |\mathbf{K}_-, \downarrow\rangle$ and $|\mathbf{K}_-, \uparrow\rangle, |\mathbf{K}_+, \downarrow\rangle$ corresponding to a symmetry breaking pattern described by Eq. (99). In both cases, switching on the Zeeman interaction leads to further splitting of the level $n = 0$ resulting in four different levels, thus completely lifting the 4-fold degeneracy of this level in noninteracting theory. For both gaps considered we expect QHE with the filling factors $\nu = 0, \pm 1, \pm 2k$ where k is a positive integer.

Let us now consider the \mathcal{P} -even, \mathcal{T} -odd gap $\Delta\bar{\Psi}\gamma^3\gamma^5\Psi$ which does not break the $U(4)$ symmetry. All Landau levels have 4-fold degeneracy. More precisely, for the levels with $n = 0$, the states of either spin from \mathbf{K}_+ - valley residing on the sublattice B are degenerate with the states of both spins from \mathbf{K}_+ - valley residing

^fWe are grateful to D.V. Khveshchenko for a discussion on Dirac masses considered in this section.

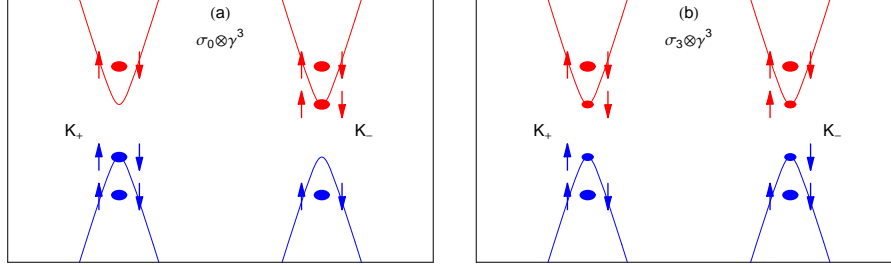


Fig. 4. (Colour online) Landau levels including spin degree of freedom, but taking zero value of Zeeman splitting. Electrons are shown in red and holes in blue. (a) for $\sigma_0 \otimes \gamma^3$ gap. (b) for $\sigma_3 \otimes \gamma^3$ gap.

on the sublattice A. Applying the Zeeman term, one now obtains only 2 different (doubly degenerate) levels.

Finally, for \mathcal{P} -even, \mathcal{T} -even gap $\Delta \bar{\Psi} \sigma_3 \gamma^3 \gamma^5 \Psi$ one has two pairs of states for the $n = 0$ Landau levels: $|\mathbf{K}_+, \uparrow\rangle, |\mathbf{K}_-, \uparrow\rangle$ and $|\mathbf{K}_+, \downarrow\rangle, |\mathbf{K}_-, \downarrow\rangle$, which remain degenerate even when the Zeeman interaction is turned on. Hence, for the last two gaps we expect QHE with the fillings factors $\nu = 2k$ with $k = 0, \pm 1, \pm 2, \dots$

4. Electromagnetic response

4.1. Electrical conductivity

The frequency-dependent electrical conductivity tensor $\sigma_{\alpha\beta}(\Omega)$ is calculated using the Kubo formula

$$\sigma_{\alpha\beta}(\Omega) = \frac{K_{\alpha\beta}(\Omega + i0)}{-i(\Omega + i0)}, \quad K_{\alpha\beta}(\Omega + i0) \equiv \frac{\langle \tau_{\alpha\beta} \rangle}{V} + \frac{\Pi_{\alpha\beta}^R(\Omega + i0)}{\hbar V}, \quad (109)$$

where the retarded correlation function for currents is given by

$$\Pi_{\alpha\beta}^R(\Omega) = \int_{-\infty}^{\infty} dt e^{i\Omega t} \Pi_{\alpha\beta}^R(t), \quad \Pi_{\alpha\beta}^R(t) = -i\theta(t) \text{Tr}(\hat{\rho}[J_\alpha(t), J_\beta(0)]), \quad (110)$$

V is the volume (area) of the system, $\hat{\rho} = \exp(-\beta H_0)/Z$ is the density matrix of the grand canonical ensemble, $\beta = 1/T$ is the inverse temperature, $Z = \text{Tr} \exp(-\beta H_0)$ is the partition function, and J_α are the total paramagnetic current operators with

$$J_\alpha(t) = e^{iHt/\hbar} J_\alpha(0) e^{-iHt/\hbar}, \quad J_\alpha(t) = \sum_{\mathbf{n}} j_\alpha^P(t, \mathbf{n}), \quad (111)$$

expressed via the paramagnetic current density (8). The diamagnetic or stress tensor $\langle \tau_{\alpha\beta} \rangle$ in the Kubo formula (109) is a thermal average of the diamagnetic part (9)

$$\langle \tau_{\alpha\beta} \rangle = \left\langle \sum_{\mathbf{n}} \tau_{\alpha\beta}(\mathbf{n}) \right\rangle. \quad (112)$$

In many cases, the effective low-energy QED₂₊₁ description provides a very good starting point for the investigation of the various transport properties of graphene

making it possible to use the powerful field theoretical methods that allow us to obtain rather simple analytical expressions. In this case, the conductivity tensor in Eq. (109) is calculated for the model Lagrangian (90) rather than the full tight-binding model in Eq. (5).

4.2. Zero field AC conductivity in the continuum Dirac model

One of the interesting results for the zero magnetic field case is that in the high-frequency limit, the interband contribution to longitudinal conductivity is constant^{97,98,99,100,101}

$$\text{Re}\sigma_{xx}(\Omega) \simeq \frac{\pi e^2}{2h}, \quad \Omega \gg |\mu|, T. \quad (113)$$

It is remarkable that the conductivity is universal, independent of the band structure parameters t and v_F . Moreover, Eq. (113) is even valid for a finite wave-vector \mathbf{k} , $kv_F \ll T \ll \Omega$.¹⁰⁰ The flatness of the conductivity results from the interband transitions between electron and hole bands at \mathbf{K}_\pm points. Of course, this result needs modification if the photon energy becomes comparable to the band edge energy, when the assumption of linear momentum dispersion relation ceases to be valid. We will return to this important question in Sec. 4.4.

A more general expression⁹⁸ for the conductivity $\sigma_{xx}(\Omega, T)$ valid in the limit of small impurity scattering rate $\Gamma(\omega)$ and neglecting the real part of the impurity self-energy reads

$$\begin{aligned} \sigma_{xx}(\Omega, T) &= \frac{e^2}{\pi^2 \hbar} \int_{-\infty}^{\infty} d\omega \frac{[n_F(\omega) - n_F(\omega')]}{\Omega} \frac{\pi}{4\omega\omega'} \\ &\times \left[\frac{2\Gamma(\omega)}{\Omega^2 + 4\Gamma^2(\omega)} - \frac{2\Gamma(\omega)}{(\omega + \omega')^2 + 4\Gamma^2(\omega)} \right] \\ &\times (|\omega| + |\omega'|)(\omega^2 + \omega'^2), \quad \omega' = \omega + \Omega. \end{aligned} \quad (114)$$

The first term in square brackets of Eq. (114) describes the intraband transitions and the second term, which reduces to Eq. (113), describes the interband transitions. An essential feature of Eq. (114) is that we kept the energy dependence of $\Gamma(\omega)$. In deriving this equation, we have assumed the small Ω limit, so that $\Gamma(\omega') \simeq \Gamma(\omega)$ and for $\Omega \ll T$, the difference $[n_F(\omega) - n_F(\omega')]/\Omega$ can be replaced by the derivative $-\partial n_F(\omega)/\partial\omega$. The intraband term of Eq. (114) in this case results in the following expression for Drude conductivity

$$\sigma_{xx}(\Omega, T) = \sigma_{00} \int_{-\infty}^{\infty} d\omega \left(-\frac{\partial n_F(\omega)}{\partial\omega} \right) \frac{2\pi|\omega|\Gamma(\omega)}{\Omega^2 + 4\Gamma^2(\omega)}, \quad (115)$$

with $\sigma_{00} = e^2/(\pi^2 \hbar)$. As discussed in Ref. 98, the frequency dependence of $\Gamma(\omega)$ could be probed by measuring $\sigma_{xx}(\Omega)$ at the different values of the gate voltage V_g .

In fact, if it is assumed that $\Gamma(\omega)$ is linear in ω , as can be expected in the Born approximation for weak scattering when the chemical potential $\mu = 0$, i.e. $\Gamma(\omega) = \gamma_{00} + \alpha|\omega|$ with a small value of γ_{00} , then one can show

$$\sigma_{xx}(\Omega, T) \simeq \frac{\pi\sigma_{00}}{2\alpha} \left[1 - \frac{\pi}{8\alpha} \frac{\Omega}{T} \right], \quad \gamma_{00} < \Omega \ll T. \quad (116)$$

Note the linear dependence on microwave frequency Ω with slope inversely proportional to the temperature. A similar formula has been derived for the microwave conductivity in a d -wave superconductor,¹⁰² a system which, as mentioned in Sec. 3.2, can also be described by QED₂₊₁. It was used to explain the cusp like behavior seen in pure samples of ortho II YBCO_{6.5} in which every second chain is complete and the others entirely missing. Eq. (115) offers the possibility of observing directly through microwave experiments the transport quasiparticle scattering rates in graphene and establishing whether the scattering is weak and the Born approximation applies, or it is strong (unitary limit) and a better model for $\Gamma(\omega)$ is constant Γ_0 within the energy range of importance in microwave experiments. In this case, Eq. (115) reduces to a Drude profile even for $\mu = 0$.

Another prediction of theory is that for $|\mu| > T$, Eq. (116) is replaced by

$$\sigma_{xx}(\Omega, T) = \sigma_{00} 2\pi |\mu| \frac{(\gamma_{00} + \alpha|\mu|)}{\Omega^2 + 4(\gamma_{00} + \alpha|\mu|)^2} \quad (117)$$

which has the Drude form and shows the remarkable property that its width can be increased continuously by increasing the gate voltage, although the impurity content is left unchanged. This arises due to the relation $\mu \propto \text{sgn } V_g \sqrt{|V_g|}$ (see Sec. 4.4.2 below), because of the increase in residual scattering which is proportional to the final state density of states which varies as $|\omega|$.

In the context of massive Dirac quasiparticles, we note that for $T = 0$ and in the limit of zero scattering $\Gamma \rightarrow 0$, one can obtain a remarkably simple form for the conductivity, viz.

$$\begin{aligned} \sigma_{xx}(\Omega) &= \frac{2\pi e^2}{h} \delta(\Omega) \frac{(\mu^2 - \Delta^2) \theta(\mu^2 - \Delta^2)}{|\mu|} \\ &+ \frac{\pi e^2}{2h} \frac{\Omega^2 + 4\Delta^2}{\Omega^2} \theta\left(\frac{|\Omega|}{2} - \max(|\mu|, \Delta)\right). \end{aligned} \quad (118)$$

Here, the theta function $\theta(|\Omega|/2 - \max(|\mu|, \Delta))$ cuts off the low Ω part of the interband contribution at $2|\mu|$ or 2Δ whichever is the largest. The expression in Eq. (118) was obtained considering as an example the excitonic gap in Eq. (93). The factor $(\Omega^2 + 4\Delta^2)/\Omega^2$ in the second term of Eq. (118) modifies the interband contribution from its constant value of the massless Dirac case. At large Ω , this modulating factor goes to 1, but for $\Omega = 2\Delta$ it is equal to 2. This shows that the existence of a finite Δ does have a clear signature in the AC conductivity. So far only ARPES measurements show some evidence for a finite value of the gap Δ at $B = 0$ in graphene epitaxially grown on SiC.¹⁰³ We will consider the situation for finite magnetic fields in the next Section.

4.3. Magneto-optical conductivity

Motivated by recent experimental advances in infrared spectroscopy of one layer graphene,²⁹ a few layer epitaxial graphite¹⁰⁴ and in highly oriented pyrolytic graphite,¹⁰⁵ we discuss some results obtained in Refs. 106, 99 for magneto-optical conductivity of graphene here. Starting from the Lagrangian (90), one can obtain a simple representation for the complex diagonal conductivity

$$\begin{aligned} \sigma_{xx}(\Omega) &= -\frac{e^2 v_F^2 |eB|}{2\pi c i} \quad (119) \\ &\times \sum_{n=0}^{\infty} \left\{ \left(1 - \frac{\Delta^2}{M_n M_{n+1}} \right) ([n_F(M_n) - n_F(M_{n+1})] + [n_F(-M_{n+1}) - n_F(-M_n)]) \right. \\ &\quad \times \frac{1}{M_{n+1} - M_n} \\ &\quad \times \left(\frac{1}{M_n - M_{n+1} + \Omega + i(\Gamma_n + \Gamma_{n+1})} - \frac{1}{M_n - M_{n+1} - \Omega - i(\Gamma_n + \Gamma_{n+1})} \right) \\ &\quad + \left(1 + \frac{\Delta^2}{M_n M_{n+1}} \right) ([n_F(-M_n) - n_F(M_{n+1})] + [n_F(-M_{n+1}) - n_F(M_n)]) \\ &\quad \times \frac{1}{M_{n+1} + M_n} \\ &\quad \times \left. \left(\frac{1}{M_n + M_{n+1} + \Omega + i(\Gamma_n + \Gamma_{n+1})} - \frac{1}{M_n + M_{n+1} - \Omega - i(\Gamma_n + \Gamma_{n+1})} \right) \right\}, \end{aligned}$$

where $M_n = \sqrt{\Delta^2 + 2nv_F^2|eB|/c}$ are the absolute values of the energies of the Landau levels.[§] The Zeeman splitting was not taken into account, because it can only shift the positions of the lines if the value of the splitting depends on Landau level index n . The Lorentzian representation (119) is derived in the Appendix of Ref. 99 using the assumption that the Landau level half-width Γ_n depends only on the Landau level index n and is independent of the energy ω . In general, the scattering rate $\Gamma_n(\omega)$ is expressed via the retarded fermion self-energy, $\Gamma_n(\omega) = -\text{Im}\Sigma_n^R(\omega)$, which depends on the energy, temperature, field and the Landau levels index n . This self-energy, which in general has a real part also, has to be determined self-consistently from the Schwinger-Dyson equation. This equation can be solved analytically^{65,107} and numerically, as was done in Refs. 16, 18. When the frequency dependence of $\text{Im}\Sigma_n^R(\omega)$ is retained, the $\text{Re}\Sigma_n^R(\omega)$ is nonzero, which results in the shift of Landau level positions. An analytical expression for the optical conductivity can also be obtained for this case.^{17,18} Similarly to Eq. (118), the expression (119) was obtained by including the excitonic gap (93).

Jiang *et al.*²⁹ have recently performed optical transmission experiment in an external field on a single layer graphene. Earlier measurements were on several layer systems, namely ultra thin epitaxial graphite.¹⁰⁴ Another recent work reported a magneto-reflectance study¹⁰⁵ of highly oriented pyrolytic graphite in a magnetic

[§]The levels with the energies $E_n = -M_n$ are explicitly included in Eq. (119) and we set $\hbar = 1$.

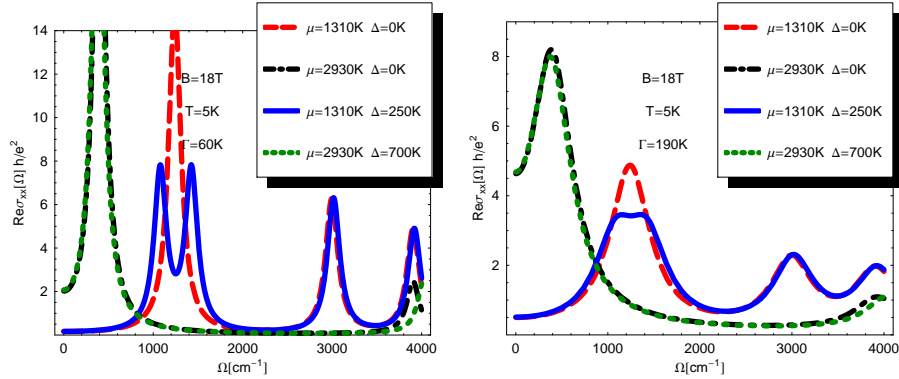


Fig. 5. (Colour online) Real part of the longitudinal conductivity, $\text{Re } \sigma_{xx}(\Omega)$ in units of e^2/h vs frequency Ω in cm^{-1} for field $B = 18 \text{ T}$, temperature $T = 5 \text{ K}$. Long dashed, the chemical potential $\mu = 1310 \text{ K}$ and the gap $\Delta = 0 \text{ K}$, dash-dotted $\mu = 2930 \text{ K}$ and $\Delta = 0 \text{ K}$, solid $\mu = 1310 \text{ K}$ and $\Delta = 250 \text{ K}$, short dashed $\mu = 2930 \text{ K}$ and $\Delta = 700 \text{ K}$. For the left frame the scattering rate $\Gamma = 60 \text{ K}$ and for the right frame scattering rate $\Gamma = 190 \text{ K}$.

field up to 18 T. In this experiment the Landau level energies are found to be linear in B , while in graphene as well as in the epitaxial graphite samples they were found to go like \sqrt{B} instead, which is consistent with Dirac quasiparticles. While this is expected in a single sheet graphene, the situation is not as clear for the multilayer case. Consequently the data in this case were analyzed in some detail in Ref. 106 and the discrepancies with our Eq. (119) were noted. In particular, it is hard to understand the observed ratio of the intensity of the first to the second interband line. We do not repeat details here, rather we comment on the newest data of Jiang *et al.*²⁹. In particular, these authors find that the distance between the Landau levels with the energies $-M_1$ and M_2 is somewhat bigger than predicted on the basis of the independent particle model such as Eq. (119). They examine the possible effect of Coulomb interaction as described by A. Iyengar *et al.*¹⁰⁸ on Landau levels and tentatively conclude that this could possibly explain the data. On the other hand, they observe that the model with a gap for the $\nu = 0$ plateau included as in Eq. (119) is not compatible with their observations, at least in the present form. It predicts a reduction rather than the observed small increase in spacing between first and second interband optical line. At this early stage, however, it is hard to be definitive about correlation effects. In Fig. 5 we show results for the real part of the longitudinal conductivity $\text{Re } \sigma_{xx}(\Omega)$ for $B = 18 \text{ T}$, $T = 5 \text{ K}$ and two possible Landau level half-width $\Gamma = 60 \text{ K}$ (roughly 4 times larger than that observed in dc measurements for $\nu = 4$ plateaux in Ref. 26) and $\Gamma = 190 \text{ K}$, which corresponds to the observed (in Ref. 29) 20 fs half-widths of the transmission peaks. We show results for two values of chemical potential $\mu = 1310 \text{ K}$ and $\mu = 2930 \text{ K}$. The first corresponds to the line T_1 in Ref. 29 measured at the filling factor $\nu = 2$ with the carrier imbalance $\rho = 9.4 \times 10^{11} \text{ cm}^{-2}$, and falls between M_0 and M_1 Landau

level energies in the notation of Eq. (119). The second corresponds to the line T_2 in Ref. 29, $\nu = 10$ with the carrier imbalance $\rho = 4.7 \times 10^{12} \text{ cm}^{-2}$ and falls between M_2 and M_3 Landau level energies.^h The long dashed (red) curve includes no gap Δ . It displays an interband absorption peak at $\Omega = 1248 \text{ cm}^{-1}$ corresponding to the transition from $n = 0$ to $n = 1$ levels, with a second at $\Omega = 3013 \text{ cm}^{-1}$ (from $-M_1$ to M_2 and $-M_2$ to M_1), a third at $\Omega = 3927 \text{ cm}^{-1}$ (from $-M_2$ to M_3 and $-M_3$ to M_2) etc. The solid (blue) line is for the same case, but now a gap $\Delta = 250 \text{ K}$ is introduced to illustrate its effect on the absorption line. We see no change in the higher energy peaks but the peak at $\Omega = 1248 \text{ cm}^{-1}$ is split into two, one shifted to lower energies and the other to higher energies. Each one is broadened by the peak half-width $2\Gamma = 120 \text{ K}$. While our parameters were chosen with the experiments of Jiang *et al.*²⁹ in mind, no splitting of the first interband line is observed, which is consistent with the fact that their Γ is considerably larger. If we increase Γ instead to their value 190 K , the results are shown in the right hand frame, which differs from the left hand counterpart only through the value of Γ . We see broader peaks associated with the various optically induced allowed transitions between Landau levels. Also, the broadening of the first interband line in the solid (blue) curve is now sufficient, so that a single peak is seen. However, it does not have the single Lorentzian lineshape of the dashed (red) line. There is a slight depression at the position of the original peak, a flat top and slight overall broadening of the line. There is no visible increase in the distance between the first and second absorption peak.

We have included in Fig. 5, for comparison, results for another value of chemical potential $\mu = 2930 \text{ K}$. This corresponds to the case when μ lies between the second and third Landau levels. As described in Ref. 106, in this instance the first interband line has faded into the background, as has the second, and the third has halved its original intensity (i.e. compared with the long dashed (red) curve). This is seen in the dash-dotted (black) curve which has $\Delta = 0$. Note that a new line appears at lower energies $\Omega = 397 \text{ cm}^{-1}$ which corresponds to an intraband transition between the second and third Landau levels. To observe even a small change in this curve in the region above $\sim 3500 \text{ cm}^{-1}$, we need to include a large gap $\Delta = 700 \text{ K}$ as seen in the dotted (green) curve.

One of the important predictions of Eq. (119) which has not been addressed yet in any of the reports on optical experiments done so far, is the behavior of the absorption lines as the chemical potential is changed. As we saw in Fig. 5 for μ falling in the energy range between $n = 0$ and $n = 1$ Landau levels, there is a line at $\Omega = M_1$. This line is anomalous in the sense that it disappears when μ falls beyond this range. If μ falls between $n = 1$ and $n = 2$, there will still be an interband line at $M_1 + M_2$, but it will have only half the intensity it had in the previous case. The

^hThe actual measurements in Ref. 29 were made for holes with $\nu = -2$ and -10 , but from theoretical consideration the particle-hole symmetry is obeyed because the conductivity (119) is an even function of μ .

other lines remain. If we further increase μ to fall between M_2 and M_3 , this would correspond to the dash-dotted (black) curve in Fig. 5 discussed above, i.e. the first and second interband lines have disappeared and the third halved its intensity.

It is hoped that future experiments will verify this predicted pattern of change with increase of μ and in particular verify that the first interband line is anomalous.¹⁰⁶ It appears at full intensity or not at all, while all other lines first fall to half intensity before disappearing entirely. Its optical spectral weight is transferred to an intraband line at $M_{n+1} - M_n$.

We note that the present consideration is based on a perfect symmetry between particles and antiparticles, which is built into the Dirac formalism. Accordingly, as we saw above, two different transitions can contribute equally to the same optical line. A most recent experiment⁴⁴ shows, however, clear evidence for the breaking of particle-antiparticle symmetry in the graphene system at the level of 2.5%, approximately five times larger than expected.

Coming back to the role of correlation effects, we mention another recent paper by Jiang *et al.*²⁸ which also points to possible limitations of an independent particle theory. Based on magnetoresistance measurements in fields up to 45 T it is concluded that the observed activation gap is much smaller than expected on the basis of the known spacing between Landau levels, which is set by the value of the Fermi velocity v_F . These results point to a need to include in the theory, additional effects which go beyond the independent particle model. In this work, we have classified and discussed several possibilities related to different Dirac masses and, as an example, considered the effect of an excitonic gap on the optical conductivity. We hope that this can help when pursuing future developments.

4.4. Sum rules for the optical and Hall conductivity

It is instructive to consider the case when QED₂₊₁ approximation is not sufficient and one should consider a full tight-binding model (5). This example is given by the optical conductivity sum rules.¹⁰⁹ The real part of the frequency dependent optical conductivity $\sigma_{xx}(\Omega)$ is its absorptive part and its spectral weight distribution as a function of energy ($\hbar\Omega$) is encoded with information on the nature of the possible electronic transitions resulting from the absorption of a photon. Even though the relationship of the conductivity to the electronic structure and transport lifetimes is not straightforward, much valuable information can be obtained from such data. In particular, the f -sum rule on the real part of $\sigma_{xx}(\Omega)$ states that (see e.g. Refs. 40, 110, 112, 111 for a review)

$$\frac{1}{\pi} \int_{-\infty}^{\infty} d\Omega \text{Re} \sigma_{xx}(\Omega) = \frac{\langle \tau_{xx} \rangle}{V}, \quad (120)$$

where $\langle \tau_{xx} \rangle$ is the thermal average of the diamagnetic term (112). The optical conductivity sum rule is a consequence of gauge invariance and causality. Gauge invariance dictates the way that the vector potential enters Eq. (5) and determines

the diamagnetic and paramagnetic terms in the expansion (6) as well as the form of Kubo formula (109). Causality implies that the conductivity, Eq. (109) satisfies the Kramers-Krönig relation. Note that defining the plasma frequency ω_P via $\omega_P^2/(4\pi)\delta_{\alpha\beta} \equiv \langle \tau_{\alpha\beta} \rangle/V$, we can rewrite the RHS of the sum rule (120) in terms of ω_P .

For a finite single tight-binding band, one can explicitly calculate the thermal average (112) and obtain the following representation of the optical sum rule^{40,110,112,111}

$$\frac{2}{\pi} \int_0^{\Omega_M} d\Omega \text{Re} \sigma_{xx}(\Omega) = \frac{e^2}{\hbar^2 V} \sum_{\mathbf{k}, \sigma} n_{\mathbf{k}, \sigma} \frac{\partial^2 \epsilon_{\mathbf{k}}}{\partial k_x^2}, \quad (121)$$

with Ω_M being a cutoff energy on the band of interest and only the contribution to $\text{Re} \sigma_{xx}(\Omega)$ of this particular band is to be included in the integral. Here $\epsilon_{\mathbf{k}}$ is the electronic dispersion, \mathbf{k} is the wave vector in the Brillouin zone, and $n_{\mathbf{k}, \sigma}$ is the probability of occupation of the state $|\mathbf{k}, \sigma\rangle$. For tight-binding dispersion with nearest neighbor hopping on a square lattice, it is easy to show that the right-hand side (RHS) of Eq. (121) reduces to e^2/\hbar^2 multiplied by minus one-half of the kinetic energy, $W_{\text{K.E.}}$ per atom.

When a constant external magnetic field is applied to a metallic system in the z -direction, the optical conductivity acquires a transverse component $\sigma_{xy}(\Omega)$ in addition to the longitudinal component $\sigma_{xx}(\Omega)$. This quantity gives additional information on the electronic properties modified by the magnetic field. In this case,¹¹³ there is a new sum rule on the optical Hall angle $\theta_H(\Omega)$. If we define

$$t_H(\Omega) \equiv \tan \theta_H(\Omega) = \frac{\sigma_{xy}(\Omega)}{\sigma_{xx}(\Omega)}, \quad (122)$$

then

$$\frac{2}{\pi} \int_0^\infty d\Omega \text{Re} t_H(\Omega) = \omega_H, \quad (123)$$

where ω_H is the Hall frequency which corresponds to the cyclotron frequency $\omega_c = eB/mc$ for free electrons.

4.4.1. Limitations of the Dirac approximation

The fact mentioned above that the effective low-energy Dirac description of graphene is insufficient for the derivation of the sum rules can be easily understood from two examples. As we have seen the RHS of Eq. (120) is normally equal to^{40,110,111,112} the thermal average of the diamagnetic term (112) that is defined as the second derivative of the Hamiltonian [see Eq. (9) above] with respect to the vector potential. This term is zero if one tries to obtain it from the approximated Dirac Lagrangian (54). On the other hand, it follows from the same Dirac approximation that, in the high-frequency limit, the interband contribution to conductivity is constant^{97,98,99,100} given by Eq. (113). The frequency Ω is unbounded in the

Dirac approximation, although physically Ω should be well below the band edge. This example indicates that when considering sum rules, one should go beyond the Dirac approximation.

The second example is that the cyclotron frequency ω_c for the Dirac quasiparticles¹⁶ is defined in a different way, $\omega_c = eBv_F^2/(c|\mu|)$, where v_F is the Fermi velocity. This definition follows from the fact that a fictitious “relativistic” mass^{14,15,17} $m_c = |\mu|/v_F^2$ plays the role of the cyclotron mass in the temperature factor of the Lifshits-Kosevich formula for graphene.^{114,115} This cyclotron frequency diverges as $\mu \rightarrow 0$, also posing the question as what one should use as a Hall frequency on the RHS of Eq. (123).

4.4.2. Diagonal conductivity sum rule

These problems were resolved in Ref. 109, where considering a tight-binding model (5) we obtained the RHS of the sum rule (120) to be equal to

$$\frac{\langle \tau_{\alpha\alpha} \rangle}{V} = \frac{2e^2}{\hbar^2} \int_{BZ} \frac{d^2\mathbf{k}}{(2\pi)^2} [n_F(\epsilon(\mathbf{k})) - n_F(-\epsilon(\mathbf{k}))] \left[\frac{\partial^2}{\partial k_\alpha^2} - \left(\frac{\partial\varphi(\mathbf{k})}{\partial k_\alpha} \right)^2 \right] \epsilon(\mathbf{k}). \quad (124)$$

Here $n_F(\omega) = 1/[\exp((\omega - \mu)/T) + 1]$ is the Fermi distribution, the phase $\varphi(\mathbf{k})$ is defined below Eq. (10) and the energy $\epsilon(\mathbf{k})$ is given by Eq. (12). The momentum integration in Eq. (124) is over the entire BZ and the thermal factors $n_F(\epsilon(\mathbf{k}))$ and $n_F(-\epsilon(\mathbf{k}))$ refer to the upper and lower Dirac cones (see Fig. 2), respectively. We stress that a simple generalization of Eq. (121) for a two band case would miss the term with the derivative of the phase, $(\partial\varphi(\mathbf{k})/\partial k_\alpha)^2$. This term occurred due to the fact that the Peierls substitution was made in the initial Hamiltonians (5) and (10) rather than after the diagonalization of Eq. (10). The second comment on Eq. (124) is that $\langle \tau_{\alpha\alpha} \rangle$ vanishes if $\epsilon(\mathbf{k})$ is taken in the linear approximation. This reflects the absence of the diamagnetic term in the Dirac approximation. The correct way is to firstly take the derivatives in Eq. (124). This leads to the final result¹⁰⁹

$$\frac{\langle \tau_{\alpha\alpha} \rangle}{V} = -\frac{e^2 a^2}{3\hbar^2} \int_{BZ} \frac{d^2\mathbf{k}}{(2\pi)^2} [n_F(\epsilon(\mathbf{k})) - n_F(-\epsilon(\mathbf{k}))] \epsilon(\mathbf{k}). \quad (125)$$

Eq. (125) is equivalent to Eq. (124). Note that $\langle \tau_{\alpha\alpha} \rangle$ is always positive and does not depend on the arbitrary choice of the sign before t in Eq. (5). Now Eq. (125) is e^2/\hbar^2 times $-2/(3\sqrt{3})(\sim -0.39)$ of the kinetic energy per atom instead of $-1/2$ for the usual square lattice.

It is useful to separate explicitly the contribution $\langle \tau_{xx}(\mu = T = 0) \rangle$ of the Dirac sea from Eq. (125):

$$\langle \tau_{xx} \rangle = \langle \tau_{xx}(\mu = T = 0) \rangle + \langle \tau_{xx}^{eh}(\mu, T) \rangle, \quad (126)$$

where

$$\frac{\langle \tau_{xx}(\mu = T = 0) \rangle}{V} = -\frac{e^2 a^2}{3\hbar^2} \int_{BZ} \frac{d^2\mathbf{k}}{(2\pi)^2} (-\epsilon(\mathbf{k})) \quad (127)$$

is the contribution of the Dirac sea (the energy of the filled valence band) and

$$\frac{\langle \tau_{xx}^{eh}(\mu, T) \rangle}{V} = -\frac{e^2 a^2}{3\hbar^2} \int_{BZ} \frac{d^2 \mathbf{k}}{(2\pi)^2} [n_F(\epsilon(\mathbf{k})) + 1 - n_F(-\epsilon(\mathbf{k}))] \epsilon(\mathbf{k}) \quad (128)$$

is the electron-hole contribution. The numerical calculation of the Dirac sea contribution (127) with the full dispersion (12) gives

$$\frac{\langle \tau_{xx}(\mu = T = 0) \rangle}{V} = \alpha \frac{e^2 t}{\hbar^2}, \quad \alpha \approx 0.61. \quad (129)$$

The same answer also follows from the linearized Dirac approximation with the trigonal density of states if the band width W is given by Eq. (42). The electron-hole contribution (128) can be estimated analytically in the linear approximation for the dispersion law. In particular, for $\mu = 0$ the temperature dependence of the diagonal conductivity sum rule is $\sim T^3$, in contrast to the often found T^2 dependence^{40,110,111,112} in tight-binding model of conventional quasiparticles.

On the other hand, for $|\mu| \gg T$ one obtains

$$\frac{\langle \tau_{xx}^{eh}(\mu, T) \rangle}{V} = -\frac{e^2 a^2}{9\pi \hbar^4 v_F^2} [|\mu|^3 + \pi^2 |\mu| T^2]. \quad (130)$$

We note that the $|\mu|^3$ behavior can be observed in an experimental configuration which has very recently been used in Ref. 29 by incorporating the specimen into a field-effect device. In this case the chemical potential μ is easily changed by varying the gate voltage V_g . Unless μ is chosen to be large, the change in the sum rule from its $\mu = 0$ value is small [$\sim (|\mu|/t)^3$]. Using Eq. (132) for carrier imbalance ρ which is proportional to V_g , we obtain that $\mu \propto \text{sgn} V_g \sqrt{|V_g|}$ and, therefore, $\langle \tau_{xx}^{eh}(V_g) \rangle / V \sim -|V_g|^{3/2}$.

4.4.3. Hall conductivity sum rule

The RHS of the Hall-angle sum rule (123) for graphene¹⁰⁹ is equal to

$$\omega_H = -\frac{1}{4\alpha} \frac{eB}{c} \frac{ta^2}{\hbar^2} \rho a^2. \quad (131)$$

Here ρ is the carrier imbalance ($\rho = n_e - n_h$), where n_e and n_h are the densities of electrons and holes, α is the numerical constant from Eq. (129). The carrier imbalance for $B = T = 0$ and in the absence of impurities is

$$\rho = \frac{\mu^2 \text{sgn} \mu}{\pi \hbar^2 v_F^2}. \quad (132)$$

Since ta^2/\hbar^2 has the dimensionality of the inverse mass and ρa^2 is dimensionless, Eq. (131) has the correct dimensionality of the Hall frequency. Substituting Eq. (132), expressing v_F via t and employing the Landau scale $L(B)$ used in Eq. (108), one can rewrite

$$\omega_H = -\frac{4 \text{sgn}(eB)}{9\pi\alpha} L^2(B) \frac{\mu^2 \text{sgn} \mu}{\hbar t^3}. \quad (133)$$

As mentioned in Sec. 4.4.1, in the recent interpretation of Shubnikov de Haas measurements, a gate voltage-dependent cyclotron mass was introduced^{14,15} through the relationship $|\mu| = m_c v_F^2$. If this is used in Eq. (133), we get

$$\omega_H = -\frac{eB}{cm_c} \left(\frac{\mu}{1.62t} \right)^3. \quad (134)$$

Since a full upper Dirac band corresponds to a value $\mu = W = \sqrt{\sqrt{3}\pi t}$ (see Eq. (42)), in this case formula (134) resembles the formula $\omega_H = \omega_c = eB/mc$ from Ref. 113 for a two-dimensional electron gas with m_c replacing the free electron mass. In graphene, however, m_c varies as the square root of the carrier imbalance $|\rho|$ and the two cases look the same only formally.

When the spectrum becomes gapped with $E = \pm\sqrt{\hbar^2 v_F^2 \mathbf{p}^2 + \Delta^2}$, where Δ is the magnitude of one of the Dirac masses (91), the carrier imbalance is

$$\rho = \frac{1}{\pi \hbar^2 v_F^2} (\mu^2 - \Delta^2) \theta(\mu^2 - \Delta^2) \text{sgn} \mu. \quad (135)$$

This implies that the gap Δ can be extracted from the change in ω_H obtained from magneto-optical measurements. This kind of measurement which reveals gapped behavior has already been done¹¹⁶ on the underdoped high-temperature superconductor $\text{YBa}_2\text{Cu}_3\text{O}_{6+x}$.

5. Conclusion

The number of articles devoted to graphene grows very fast and the seminal experimental papers where the IQHE was reported^{14,15} have already been cited almost 300 times in arXiv, while the total list of references of our review has about 100 papers. This is partly caused by the restriction on the size of the manuscript and by the amount of time we decided to invest in this project. We intentionally omitted such interesting and important topics as bilayer and multilayer graphene, the role of impurities, defects and their gauge field description, minimal conductivity at the Dirac point, edge states, weak (anti)localization, fractional quantum Hall effect, graphene nanoribbons, etc. Each of these topics may, in the future, become a subject of a review on its own. Instead we decided to restrict ourselves to the specific topics covered in the review and to discuss them in detail. We hope that this choice is indeed complementary to already existing textbooks and reviews.^{19,23,36,37}

During our work on the review, we found that in the literature on graphene, the word “*chirality*” is becoming as fashionable as “*Berry’s phase*”, but depending on researcher’s background, it is used to denote different concepts, so that it is getting hard to grasp its meaning. Here we followed the commonly accepted definition in field theory⁷⁵ and demonstrated that the chirality quantum number corresponds to the valley index in graphene. In Sec. 3.4 we also introduced the *pseudohelicity* which characterizes the projection of a quasiparticle pseudospin on the direction of its momentum and explained it specifically in 2+1 dimension and the relationship

between pseudohelicity and chirality. We hope that this solid state reincarnation of chirality will lead, in future, to a deeper understanding of chirality in field theory.

It is also very instructive to see how the spinors emerge from the two atom per unit cell description of graphene. Because these spinors are not related to a real spin, the corresponding degree of freedom is called pseudospin. This solid state realization of pseudospin may help us understand the origin of a real spin better.

Also we mentioned a link between the QED₂₊₁ description of graphene and d -wave superconductivity. In both cases, the low-energy quasiparticle excitations are described by massless QED₂₊₁. Massless excitations in graphene are often compared with massless neutrinos. However, as we pointed out in Sec. 3.5.4, this analogy is not complete, because their discrete symmetries are different. Massless QED₂₊₁ has $U(4)$ symmetry and a rather common way in the field theory to break this symmetry is a dynamical generation of the Dirac mass. It is unclear at this stage whether this rather generic mechanism works in graphene or the observed new ± 1 QHE states can be explained by other mechanisms. From our point of view, this is one of the most interesting open questions which demands further experimental and theoretical work. Accordingly, in our review we simply tried to facilitate the future theoretical work by providing a classification for possible Dirac masses.

Acknowledgements

We thank D. Basov, L. Benfatto, L. Brey, A.K. Geim, M.O. Goerbig, E.V. Gorbar, E. Henriksen, I.F. Herbut, P.I. Holod, A. Iyengar, P. Kim, D.V. Khveshchenko, Z. Li, V.M. Loktev, A.H. MacDonald, V.A. Miransky, I.A. Shovkovy and M.A.H. Vozmediano for illuminating discussions. The work of V.P.G. was supported by the SCOPES-project IB 7320-110848 of the Swiss NSF, the grant 10/07-N "Nanostructure systems, nanomaterials, nanotechnologies", and by the Program of Fundamental Research of the Physics and Astronomy Division of the National Academy of Sciences of Ukraine and by Ukrainian State Foundation for Fundamental Research. J.P.C. and S.G.Sh. were supported by the Natural Science and Engineering Research Council of Canada (NSERC) and by the Canadian Institute for Advanced Research (CIFAR). S.G.Sh. is also grateful to the Kavli Institute for Theoretical Physics at the University of California Santa Barbara (the National Science Foundation under Grant No. PHY05-51164) for hospitality during its graphene workshop.

Appendix A. Solution of the Dirac equation in the Landau gauge

The Dirac equation in symmetric gauge and in the representation (52) is solved, for example, in Appendix D of the second paper in Ref. 17 (see also Ref. 117 for a solution of 3D Dirac equation in the Landau and symmetric gauges). For $eB, \Delta > 0$ in the Landau gauge $\mathbf{A} = (0, Bx)$ the positive ($\psi_{\mathbf{K}_+}^{(+)}$) and negative ($\psi_{\mathbf{K}_+}^{(-)}$) energy

42 V.P. GUSYNIN, S.G. SHARAPOV, J.P. CARBOTTE

solutions of Eq. (104) at \mathbf{K}_+ point are

$$\begin{aligned}\psi_{\mathbf{K}_+}^{(+)}(x, y; n, p) &= \frac{1}{\sqrt{2\pi l}} e^{-i|E_n|t+ipy} \frac{1}{\sqrt{2|E_n|}} \begin{pmatrix} \sqrt{|E_n| + \Delta} w_{n-1}(\xi) \\ i\sqrt{|E_n| - \Delta} w_n(\xi) \end{pmatrix}, \quad n \geq 1, \\ \psi_{\mathbf{K}_+}^{(-)}(x, y; n, p) &= \frac{1}{\sqrt{2\pi l}} e^{i|E_n|t+ipy} \frac{1}{\sqrt{2|E_n|}} \begin{pmatrix} \sqrt{|E_n| - \Delta} w_{n-1}(\xi) \\ -i\sqrt{|E_n| + \Delta} w_n(\xi) \end{pmatrix}, \quad n \geq 1, \\ \psi_{\mathbf{K}_+}^{(-)}(x, y; n = 0, p) &= \frac{1}{\sqrt{2\pi l}} e^{i|E_0|t+ipy} \begin{pmatrix} 0 \\ -iw_0(\xi) \end{pmatrix}, \quad n = 0.\end{aligned}\quad (\text{A.1})$$

The solutions of Eq. (105) at \mathbf{K}_- point are

$$\begin{aligned}\psi_{\mathbf{K}_-}^{(+)}(x, y; n = 0, p) &= \frac{1}{\sqrt{2\pi l}} e^{-i|E_0|t+ipy} \begin{pmatrix} 0 \\ iw_0(\xi) \end{pmatrix}, \quad n = 0, \\ \psi_{\mathbf{K}_-}^{(+)}(x, y; n, p) &= \frac{1}{\sqrt{2\pi l}} e^{-i|E_n|t+ipy} \frac{1}{\sqrt{2|E_n|}} \begin{pmatrix} \sqrt{|E_n| - \Delta} w_{n-1}(\xi) \\ i\sqrt{|E_n| + \Delta} w_n(\xi) \end{pmatrix}, \quad n \geq 1, \\ \psi_{\mathbf{K}_-}^{(-)}(x, y; n, p) &= \frac{1}{\sqrt{2\pi l}} e^{i|E_n|t+ipy} \frac{1}{\sqrt{2|E_n|}} \begin{pmatrix} -\sqrt{|E_n| + \Delta} w_{n-1}(\xi) \\ i\sqrt{|E_n| - \Delta} w_n(\xi) \end{pmatrix}, \quad n \geq 1.\end{aligned}\quad (\text{A.2})$$

Here $\xi = x/l + pl$, where $l \equiv (\hbar c/|eB|)^{1/2}$ is the magnetic length and p is the momentum along the y axis,

$$E_n = \pm \sqrt{\Delta^2 + \hbar v_F^2 2n|eB|/c}, \quad (\text{A.3})$$

$$w_n(\xi) = (\pi^{1/2} 2^n n!)^{-1/2} e^{-\xi^2/2} H_n(\xi), \quad \int_{-\infty}^{\infty} d\xi w_n(\xi) w_m(\xi) = \delta_{nm}$$

with $H_n(\xi)$ being the Hermite polynomial and we defined $w_{-1}(\xi) \equiv 0$. The lowest Landau level $n = 0$ is special: while at $n \geq 1$, there are solutions corresponding to both electron ($E_n > 0$) and hole ($E_n < 0$) states at both \mathbf{K}_+ and \mathbf{K}_- points, the solution with $n = 0$ describes holes at \mathbf{K}_+ and electrons at \mathbf{K}_- point. The corresponding structure of Landau levels is shown in Fig. 3 (c). See also Fig. 2 of Ref. 118 for a graphical representation of the dependence of the LLL position on the relative signs of eB and Δ . One can also say that for $eB > 0$ the solution of Eq. (104) for LLL at \mathbf{K}_+ describes holes that live on the B sublattice, while the solution of Eq. (105) for LLL at \mathbf{K}_- corresponds to electrons living on the A sublattice (we remind that in the \mathbf{K}_- valley, the spinor components are inverted in comparison to the spinor in the \mathbf{K}_+ valley). Finally, we notice that the relation in Eq. (34) is violated in the finite field. Indeed

$$\tau_2 \mathcal{H}_0^*(k, eB) \tau_2 = -\mathcal{H}_0(k, -eB), \quad \mathcal{H}_0(k, eB) = \tau_1 k_x + \tau_2 (k_y + eBx) + \Delta \tau_3. \quad (\text{A.4})$$

This indicates that the wave function $\tau_2 |\psi\rangle^*$ is the solution of the equation $\mathcal{H}_0(k, -eB) \tau_2 |\psi\rangle^* = -E \tau_2 |\psi\rangle^*$, i.e. the generalization (A.4) of the relation (34) for a finite magnetic field does not describe the symmetry of the spectrum about $E = 0$, but rather relates the solutions of Eqs. (104) and (105) obtained for $eB > 0$ with the solutions of the same equations for $eB < 0$.

References

1. G.W. Semenoff, *Phys. Rev. Lett.* **53**, 2449 (1984).
2. K.S. Novoselov, A.K. Geim, S.V. Morozov, D. Jiang, Y. Zhang, S.V. Dubonos, I.V. Grigorieva, and A.A. Firsov, *Science* **306**, 666 (2004); K.S. Novoselov, D. Jiang, T. Booth, V.V. Khotkevich, S.M. Morozov, and A.K. Geim, *Proc. Nat. Acad. Sc.* **102**, 10451 (2005).
3. E. Fradkin, E. Dagotto, and D. Boyanovsky, *Phys. Rev. Lett.* **57**, 2967 (1986), *ibid* **58**, 961(E) (1987); D. Boyanovsky, E. Dagotto, and E. Fradkin, *Nucl. Phys. B* **285**[FS19], 340 (1987).
4. F.D.M. Haldane, *Phys. Rev. Lett.* **61**, 2015 (1988).
5. A.M.J. Schakel, *Phys. Rev. D* **43**, 1428 (1991).
6. J. González, F. Guinea, and M.A.H. Vozmediano, *Nucl. Phys. B* **406**, 771 (1993); *ibid.* **424**, 595 (1994).
7. J. González, F. Guinea, and M.A.H. Vozmediano, *Phys. Rev. Lett.* **77**, 3589 (1996); *Phys. Rev. B* **59**, R2474 (1999); *Phys. Rev. B* **63**, 134421 (2001).
8. D.V. Khveshchenko, *Phys. Rev. Lett.* **87**, 206401 (2001); *ibid.* **87**, 246802 (2001).
9. E.V. Gorbar, V.P. Gusynin, V.A. Miransky, and I.A. Shovkovy, *Phys. Rev. B* **66**, 045108 (2002).
10. A.W.W. Ludwig, M.P.A. Fisher, R. Shankar and G. Grinstein, *Phys. Rev. B* **50**, 7526 (1994).
11. C.-Y. Hou, C. Chamon, C. Mudry, *Phys. Rev. Lett.* **98**, 186809 (2007).
12. R. Jackiw and S.-Y. Pi, *Phys. Rev. Lett.* **98**, 266402 (2007).
13. I.F. Herbut, arXiv:0704.2234.
14. K.S. Novoselov, A.K. Geim, S.V. Morozov, D. Jiang, M.I. Katsnelson, I.V. Grigorieva, S.V. Dubonos, and A.A. Firsov, *Nature* **438**, 197 (2005).
15. Y. Zhang, Y.-W. Tan, H.L. Stormer, and P. Kim, *Nature* **438**, 201 (2005).
16. Y. Zheng and T. Ando, *Phys. Rev. B* **65**, 245420 (2002).
17. V.P. Gusynin and S.G. Sharapov, *Phys. Rev. Lett.* **95**, 146801 (2005); *Phys. Rev. B* **73**, 245411 (2006).
18. N.M.R. Peres, F. Guinea, and A.H. Castro Neto, *Phys. Rev. B* **73**, 125411 (2006).
19. A.K. Geim and K.S. Novoselov, *Nature Materials* **6**, 183 (2007).
20. K.S. Novoselov, Z. Jiang, Y. Zhang, S.V. Morozov, H.L. Stormer, U. Zeitler, J.C. Maan, G.S. Boebinger, P. Kim, and A.K. Geim, *Science* **315**, 1379 (2007).
21. M.I. Katsnelson, K. S. Novoselov and A.K. Geim, *Nature Phys.* **2**, 620 (2006).
22. A. Calogeracos, *Nature Phys.* **2**, 579 (2006).
23. M.I. Katsnelson and K.S. Novoselov, *Solid State Comm.* **143**, 3 (2007).
24. J. Cserti and G. Dávid, *Phys. Rev. B* **74**, 172305 (2006).
25. X. Wu, X. Li, Z. Song, C. Berger, and W.A. de Heer, *Phys. Rev. Lett.* **98**, 136801 (2007).
26. Y. Zhang, Z. Jiang, J.P. Small, M.S. Purewal, Y.-W. Tan, M. Fazlollahi, J.D. Chudow, J.A. Jaszczak, H.L. Stormer, and P. Kim, *Phys. Rev. Lett.* **96**, 136806 (2006).
27. D.A. Abanin, K.S. Novoselov, U. Zeitler, P.A. Lee, A.K. Geim, L.S. Levitov, *Phys. Rev. Lett.* **98**, 196806 (2007).
28. Z. Jiang, Y. Zhang, Y. Tan, H. Stormer, and P. Kim, *Phys. Rev. Lett.* **99**, 106802 (2007).
29. Z. Jiang, E.A. Henriksen, L.C. Tung, Y.-J. Wang, M.E. Schwartz, M.Y. Han, P. Kim, and H.L. Stormer, *Phys. Rev. Lett.* **98**, 197403 (2007).
30. W. Kohn, *Phys. Rev.* **123**, 1241 (1961).
31. K. Yang, *Solid State Comm.* **143**, 27 (2007).
32. M. Wilson, *Phys. Today*, January 2006, 21.

44 V.P. GUSYNIN, S.G. SHARAPOV, J.P. CARBOTTE

33. A.H. Castro Neto, F. Guinea, and N.M. Peres, *Physics World* **19**, 33 November (2006).
34. T. Chakraborty, *Physics in Canada* **62**, 351 (2006).
35. M.I. Katsnelson, *Mater. Today* **10**, Issue 1&2, 20 (2007).
36. R. Saito, G. Dresselhaus and M.S. Dresselhaus, *Physical Properties of Carbon Nanotubes*, Imperial College Press, London, 1998.
37. T. Ando, *J. Phys. Soc. Jpn.* **74**, 777 (2005).
38. W.H. Lomer, *Proc. Roy. Soc.* **A227**, 330 (1955).
39. J.C. Slonczewski and P.R. Weiss, *Phys. Rev.* **109**, 272 (1958).
40. A. J. Millis, in *Strong Interactions in Low Dimensions*, edited by D. Baeriswyl and L. De Giorgi (Kluwer Academic, Berlin, 2003).
41. J.C. Meyer, A.K. Geim, M.I. Katsnelson, K.S. Novoselov, T.J. Booth, and S. Roth, *Nature* **446**, 60 (2007).
42. H. Fukuyama, *J. Phys. Soc. Jpn.* **76** 043711 (2007).
43. P.R. Wallace, *Phys. Rev.* **77**, 622 (1947).
44. R.S. Deacon, K-C. Chuang, R.J. Nicholas, K.S. Novoselov, and A.K. Geim, *Phys. Rev. B* **76**, 081406(R) (2007).
45. J.L. Mañes, F. Guinea, and M.A.H. Vozmediano, *Phys. Rev. B* **75**, 155424 (2007).
46. Y. Hatsugai, T. Fukui, and H. Aoki, cond-mat/0701431.
47. G. Giovannetti, P.A. Khomyakov, G. Brocks, P.J. Kelly, and J. van den Brink, *Phys. Rev. B* **76**, 073103 (2007).
48. A.S. Davydov, *Quantum Mechanics*, 2nd Edition, Pergamon, New York, 1976.
49. S. Ryu and Y. Hatsugai, *Phys. Rev. Lett.* **89**, 077002 (2002).
50. K. Ziegler, cond-mat/0703628.
51. G.E. Volovik, in *Quantum Analogues: From Phase Transitions to Black Holes and Cosmology*, Eds. W.G. Unruh and R. Schutzhold, Springer Lecture Notes in Physics 718/2007, pp. 31-73; cond-mat/0601372.
52. Yu.B. Gaididei and V.M. Loktev, *Fiz. Nizk. Temp.* **32**, 923 (2006) [*Low Temp. Phys.* **32**, 703 (2006).]
53. D.P. DiVincenzo and E.J. Mele, *Phys. Rev. B* **29**, 1685 (1984).
54. H. Leal and D.V. Khveshchenko, *Nucl. Phys. B* **687**, 323 (2004); D.V. Khveshchenko and W.F. Shively, *Phys. Rev. B* **73**, 115104 (2006).
55. V.P. Gusynin, V.A. Miransky, S.G. Sharapov, and I.A. Shovkovy, *Phys. Rev. B* **74**, 195429 (2006); cond-mat/0612488.
56. I.F. Herbut, *Phys. Rev. Lett.* **97**, 146401 (2006); *Phys. Rev. B* **75**, 165411 (2007).
57. E. McCann and V.I. Fal'ko, *J. Phys.: Condens. Matter.* **16**, 2371 (2004).
58. C.L. Kane and E.J. Mele, *Phys. Rev. Lett.* **95**, 146802 (2005); *ibid.* **95**, 226801 (2005).
59. V.V. Cheianov and V.I. Fal'ko, *Phys. Rev. Lett.* **97**, 226801 (2006); *Phys. Rev. B* **74**, 041403(R) (2006).
60. E. McCann, K. Kechedzhi, V.I. Fal'ko, H. Suzuura, T. Ando, and B.L. Altshuler, *Phys. Rev. Lett.* **97**, 146805 (2006).
61. P.M. Ostrovsky, I.V. Gornyi, and A.D. Mirlin, *Phys. Rev. B* **74**, 235443 (2006).
62. D.V. Khveshchenko, *Phys. Rev. B* **75**, 153405 (2007).
63. G.E. Volovik, *Phys. Rep.* **351**, 195 (2001).
64. O. Vafek, A. Melikyan, M. Franz, and Z. Tešanović, *Phys. Rev. B* **63**, 134509 (2001); M. Franz, Z. Tešanović, and O. Vafek, *Phys. Rev. B* **66**, 054535 (2002).
65. D.V. Khveshchenko and J. Paaske, *Phys. Rev. Lett.* **86**, 4672 (2001).
66. I.F. Herbut, *Phys. Rev. B* **66**, 094504 (2002).
67. V.P. Gusynin and V.A. Miransky, *Eur. Phys. J. B* **37**, 363 (2004).
68. S.G. Sharapov and J.P. Carbotte, *Phys. Rev. B* **73**, 094519 (2006).
69. J. Alicea and M.P.A. Fisher, *Phys. Rev. B* **74**, 075422 (2006).

70. D.V. Khveshchenko, *Phys. Rev. B* **74**, 161402R (2006).
71. E.G. Mishchenko, *Phys. Rev. Lett.* **98**, 216801 (2007).
72. Y. Barlas, T. Pereg-Barnea, M. Polini, R. Asgari, and A.H. MacDonald, *Phys. Rev. Lett.* **98**, 236601 (2007).
73. T. Appelquist, M. Bowick, D. Karabali and L.C.R. Wijewardhana, *Phys. Rev. D* **33**, 3704 (1986).
74. T. Ando, T. Nakanishi, and R. Saito, *J. Phys. Soc. Jpn.* **67**, 2857 (1998); H. Suzuura and T. Ando, *Phys. Rev. Lett.* **89**, 266603 (2002).
75. C. Itzykson and J.-B. Zuber, *Quantum Field Theory*, McGraw-Hill Inc., 1980.
76. B. Binengar, *J. Math. Phys.* **23**, 1511 (1981).
77. D. Boyanovsky, R. Blankenbecler and R. Yahalon, *Nucl. Phys. B.* **270**, 483 (1986).
78. P.L. McEuen, M. Bockrath, D.H. Cobden, Y.-G. Yoon, and S.G. Louie, *Phys. Rev. Lett.* **83**, 5098 (1999).
79. R. Jackiw and S. Templeton, *Phys. Rev. D* **23**, 2291 (1981).
80. Y. Hosotani, *Phys. Lett. B* **319**, 332 (1993); *Phys. Rev. D* **51**, 2022 (1995).
81. A. Altland, B.D. Simons and M.R. Zirnbauer, *Phys. Rep.* **359**, 283 (2002).
82. A.M. Garcia-Garcia and E. Cuevas, *Phys. Rev. B* **74**, 113101 (2006).
83. O. Tchernyshyov, *Phys. Rev. B* **62**, 16751 (2000).
84. H.B. Heersche, P. Jarillo-Herrero, J.B. Oostinga, L.M.K. Vandersypen and A.F. Morpurgo, *Nature* **446**, 56 (2007).
85. M. Titov and C.W.J. Beenakker, *Phys. Rev. B* **74**, 041401(R) (2006).
86. D.A. Abanin, P.A. Lee, and L.S. Levitov, *Phys. Rev. Lett.* **96**, 176803 (2006), *ibid.* **98**, 156801 (2007); *Solid State Comm.* **143**, 77 (2007).
87. K. Nomura and A. H. MacDonald, *Phys. Rev. Lett.* **96**, 256602 (2006).
88. K. Yang, S. Das Sarma, and A. H. MacDonald, *Phys. Rev. B* **74**, 075423 (2006).
89. M.O. Goerbig, R. Moessner, and B. Douçot, *Phys. Rev. B* **74**, 161407(R) (2006).
90. J.-N. Fuchs and P. Lederer, *Phys. Rev. Lett.* **98**, 016803 (2007).
91. M. Ezawa, cond-mat/0606084; cond-mat/0609612.
92. I.F. Herbut, *Phys. Rev. B* **76**, 085432 (2007).
93. L. Sheng, D.N. Sheng, F.D.M. Haldane, L. Balents, arXiv:0706.0371.
94. V.P. Gusynin, V.A. Miransky, and I.A. Shovkovy, *Phys. Rev. Lett.* **73**, 3499 (1994); *Phys. Rev. D* **52**, 4718 (1995); *Nucl. Phys. B* **462**, 249 (1996).
95. Y. Kopelevich, V.V. Lemanov, S. Moehlecke, and J. H. S. Torres, *Fiz. Tverd. Tela* **41**, 2135 (1999) [*Phys. Solid State* **41**, 1959 (1999)]; H. Kempa, Y. Kopelevich, F. Mrowka, A. Setzer, J. H. S. Torres, R. Höhne, and P. Esquinazi, *Solid State Commun.* **115**, 539 (2000); M. S. Sercheli, Y. Kopelevich, R. R. da Silva, J. H. S. Torres, and C. Rettori, *Solid State Commun.* **121**, 579 (2002). For the latest results of this group, see Y. Kopelevich, J. C. Medina Pantoja, R. R. da Silva, F. Mrowka, and P. Esquinazi, *Phys. Lett. A* **355**, 233 (2006).
96. E.V. Gorbar, V.P. Gusynin, V.A. Miransky, and I.A. Shovkovy, *Phys. Lett. A* **313**, 472 (2003).
97. T. Ando, Y. Zheng, and H. Suzuura *J. Phys. Soc. Jpn.* **71**, 1318 (2002).
98. V.P. Gusynin, S.G. Sharapov and J.P. Carbotte, *Phys. Rev. Lett.* **96**, 256802 (2006).
99. V.P. Gusynin, S.G. Sharapov and J.P. Carbotte, *J. Phys.: Condens. Matter.* **19**, 026222 (2007).
100. L.A. Falkovsky and A.A. Varlamov, *Eur. Phys. J. B* **56**, 281 (2007).
101. S. Ryu, C. Mudry, A. Furusaki, and A.W.W. Ludwig, *Phys. Rev. B* **75**, 205344 (2007).
102. W. Kim, F. Marsiglio, and J. P. Carbotte, *Phys. Rev. B* **70**, 060505(R) (2004).
103. A. Lanzara, private communication and S.Y. Zhou, G.-H. Gweon, A.V. Fedorov, P.N.

46 V.P. GUSYNIN, S.G. SHARAPOV, J.P. CARBOTTE

- First, W.A. de Heer, D.-H. Lee, F. Guinea, A.H. Castro Neto, and A. Lanzara, *Nature Materials* **6**, 770 (2007).
104. M.L. Sadowski, G. Martinez, M. Potemski, C. Berger, and W.A. de Heer, *Phys. Rev. Lett.* **97**, 266405 (2006); *Solid State Comm.* **143**, 123 (2007).
 105. Z.Q. Li, S.-W. Tsai, W.J. Padilla, S.V. Dordevic, K.S. Burch, Y.J. Wang, and D.N. Basov, *Phys. Rev. B* **74**, 195404 (2006).
 106. V.P. Gusynin, S.G. Sharapov and J.P. Carbotte, *Phys. Rev. Lett.* **98**, 157402 (2007).
 107. B. Dóra and P. Thalmeier, *Phys. Rev. B* **76**, 035402 (2007).
 108. A. Iyengar, J. Wang, H.A. Fertig, and L. Brey, *Phys. Rev. B* **75**, 125430 (2007).
 109. V.P. Gusynin, S.G. Sharapov and J.P. Carbotte, *Phys. Rev. B* **75**, 165407 (2007).
 110. D. van der Marel, in *Strong Interactions in Low Dimensions, Series: Physics and Chemistry of Materials with Low-Dimensional Structures*, Vol. 25, edited by D. Baeriswyl and L. De Giorgi, (Kluwer Academic, Berlin, 2005); arXiv:cond-mat/0301506.
 111. L. Benfatto and S. Sharapov, *Fiz. Nizk. Temp.* **32**, 700 (2006) [*Low Temp. Phys.* **32**, 533 (2006).]
 112. J.P. Carbotte and E. Schachinger, *J. Low Temp. Phys.* **144**, 61 (2006).
 113. H.D. Drew and P. Coleman, *Phys. Rev. Lett.* **78**, 1572 (1997).
 114. S.G. Sharapov, V.P. Gusynin, and H. Beck, *Phys. Rev. B* **69**, 075104 (2004).
 115. V.P. Gusynin and S.G. Sharapov, *Phys. Rev. B* **71**, 125124 (2005).
 116. L.B. Rigal, D.C. Schmadel, H.D. Drew, B. Maiorov, E. Osquigil, J.S. Preston, R. Hughes, and G.D. Gu, *Phys. Rev. Lett.* **93**, 137002 (2004).
 117. D.B. Melrose and A.J. Parle, *Aust. J. Phys.* **36**, 755 (1983).
 118. B.A. Bernevig, T.L. Hughes, H.-D. Chen, C. Wu, S.-C. Zhang, *Int. J. Mod. Phys. B* **20**, 3257 (2006).